
MGD: MOMENT GUIDED DIFFUSION FOR MAXIMUM ENTROPY GENERATION

A PREPRINT

Etienne Lempereur¹, Nathanaël Cuvelle–Magar¹, Florentin Coeurdoux², Stéphane Mallat^{3,4}, and Eric Vanden-Eijnden^{5,6}

¹Département d’informatique, ENS, Université PSL, Paris, France

²Capital Fund Management, Paris, France

³Collège de France, Paris, France

⁴Flatiron Institute, New York, USA

⁵Courant Institute of Mathematical Sciences, New York University, New York, USA

⁶ML Lab, Capital Fund Management, Paris, France

February 20, 2026

ABSTRACT

Generating samples from limited information is a fundamental problem across scientific domains. Classical maximum entropy methods provide principled uncertainty quantification from moment constraints but require sampling via MCMC or Langevin dynamics, which typically exhibit exponential slowdown in high dimensions. In contrast, generative models based on diffusion and flow matching efficiently transport noise to data but offer limited theoretical guarantees and can overfit when data is scarce. We introduce Moment Guided Diffusion (MGD), which combines elements of both approaches. Building on the stochastic interpolant framework, MGD samples maximum entropy distributions by solving a stochastic differential equation that guides moments toward prescribed values in finite time, thereby avoiding slow mixing in equilibrium-based methods. We formally obtain, in the large-volatility limit, convergence of MGD to the maximum entropy distribution and derive a tractable estimator of the resulting entropy computed directly from the dynamics. Applications to financial time series, turbulent flows, and cosmological fields using wavelet scattering moments yield estimates of negentropy for high-dimensional multiscale processes.

1 Introduction

Generating new realizations of a random variable $X \in \mathbb{R}^d$ from limited information arises across scientific domains, from synthesizing physical fields in computational science to creating scenarios for risk assessment in quantitative finance. Many approaches to this problem have been proposed, but two stand out for their success: the classical maximum entropy framework introduced by Jaynes [1] when moment information is available, and the modern generative modelling approach with deep neural networks [2–8] that operate when raw data samples can be accessed. These approaches take different perspectives on the problem—principled uncertainty quantification versus flexible distribution learning—suggesting potential benefits from blending both.

The maximum entropy approach provides principled uncertainty quantification when the available information consists of moments $\mathbb{E}[\phi(X)] \in \mathbb{R}^r$ for a specified moment function (or observable) $\phi : \mathbb{R}^d \rightarrow \mathbb{R}^r$. Jaynes’ principle selects the unique distribution that maximizes entropy, if it exists. It is the least committal choice consistent with available information. It provides principled protection against overfitting: generated samples are diverse within the constraint set but do not hallucinate correlations beyond what ϕ captures. This is particularly valuable when data is scarce. This maximum entropy distribution has an exponential density $p_{\theta_*}(x) = \mathcal{Z}_{\theta_*}^{-1} e^{-\theta_*^T \phi(x)}$, where θ_* are Lagrange multipliers and \mathcal{Z}_{θ_*} is the normalisation constant. While theoretically elegant and providing rigorous control over uncertainty, this approach is not a generative model *per se*. Classical maximum entropy estimation [9–11] requires sampling from intermediate distributions.

tributions to compute log-likelihood gradients, both for estimating the Lagrange multipliers θ_* and for generating samples from p_{θ_*} . Unfortunately, samplers based on MCMC or on a Langevin equation suffer from critical slowing down [12, 13]: sampling becomes prohibitively expensive in high dimension for non-convex Gibbs energies $\theta_*^T \phi(x)$.

Recent generative modelling approaches emphasize flexible distribution learning when samples $(x^i)_{i \leq n}$ are available. Modern generative models—notably score-based diffusion [6–8] and flow matching with stochastic interpolants [3, 4, 14]—learn to sample from an approximation of the underlying distribution by transporting Gaussian noise to data samples along carefully designed paths using Ordinary Differential Equations (ODE) or Stochastic Differential Equations (SDE), with a drift estimated by quadratic regression with a neural network. This transport avoids the exponential scaling with barrier heights that plagues classical MCMC and Langevin sampling. However, this flexibility comes at a cost: they provide no explicit control over statistical moments and their approximation error remains theoretically uncontrolled, making them prone to overfitting when data is scarce [15].

We introduce a Moment Guided Diffusion (MGD), which blends both paradigms. MGD samples maximum entropy distributions when data samples are available, using a transport that guides moments estimated from these data. To achieve this, MGD relies on two key ingredients. First, it uses a diffusive process X_t whose moments match those of a stochastic interpolant I_t that continuously transforms Gaussian noise into data: $\mathbb{E}[\phi(X_t)] = \mathbb{E}[\phi(I_t)]$ for all $t \in [0, 1]$. This diffusion steers the distribution of the process from noise to data along a homotopic path, achieving non-equilibrium transport in finite time and avoiding the critical slowing down that plagues classical Langevin dynamics. Second, the SDE includes a tunable volatility σ that controls convergence to the maximum entropy distribution. As σ increases, under appropriate assumptions we prove that the process converges to the maximum entropy among all distributions satisfying the moment constraints. We conjecture that this convergence occurs at rate $O(\sigma^{-2})$, and provide numerical verification.

MGD also enables estimation of the entropy of the resulting distribution. We provide a tractable lower bound on the maximum entropy, computed directly from the MGD dynamics. We conjecture and numerically validate that this lower bound converges at rate $O(\sigma^{-2})$. This allows us to calculate the negentropy, which measures the non-Gaussianity of a random process as the difference between the entropy of a Gaussian with the same covariance and the entropy of the process [16, 17]. Prior to this work, numerical computation of this information-theoretic measure was prohibitively expensive for high-dimensional processes characterized by non-convex energies.

The MGD SDE is a nonlinear (McKean-Vlasov) equation whose drift depends on moments of its own solution.

These moments are estimated empirically using interacting particles, and the dynamics is discretized in time. The computational cost scales as $O(\sigma^2)$, with a constant independent of both the data dimension and the non-convexity of the Gibbs energy.

MGD is related to microcanonical sampling algorithms [18], which also generate samples in high dimension without estimating Lagrange parameters. However, the two methods differ in important ways. Microcanonical algorithms transport a Gaussian distribution toward a distribution satisfying the moment constraints using a gradient descent on the moment mismatch, which requires infinite time. Despite good numerical results in high dimension [19–21], they are not guaranteed to converge to the maximum entropy distribution, nor can they estimate the maximum entropy value. MGD, by contrast, achieves finite-time transport along a homotopic path and provides a tractable entropy estimator.

We apply MGD to high-dimensional multiscale stochastic processes, generating financial time-series and physical fields from maximum entropy models conditioned by wavelet scattering moments [18, 21]. MGD produces accurate models of complex non-Gaussian processes with long-range correlations, including financial time series (S&P 500), turbulent flows [22], and cosmological fields [23]. For these fields, we provide the first estimates of negentropy.

The remainder of this paper is organized as follows. Section 2 reviews classical maximum entropy sampling via MCMC and Langevin dynamics, as well as modern generative models based on diffusion and stochastic interpolants. Section 3 introduces the MGD transport and its numerical implementation. Section 4 presents the entropy estimator, discusses the convergence of MGD as the volatility increases, and states our conjectures on the convergence rate. Section 5 provides numerical verification of these conjectures. Section 6 applies MGD to high-dimensional multiscale processes—financial time series, turbulent flows, and cosmological fields—using wavelet scattering moments, and estimates their negentropy. Technical proofs and additional details are provided in Appendix.

2 Background: Classical Maximum Entropy and Modern Generative Modeling

We review the classical sampling approach of maximum entropy distributions with Langevin dynamics (Section 2.1) and modern generative modeling based on transport via flow matching and stochastic interpolants (Section 2.2).

Table 1: Comparison of sampling approaches for complex distributions.

Approach	Input	Max-ent guarantee	Moment control	Sampling
Maximum entropy (classical)	Moments m	✓	✓	Equilibrium (MCMC)
Diffusion models	Dataset (x^i)	✗	✗	Non-equilibrium
Moment Guided Diffusion	Dataset (x^i)	✓	✓	Non-equilibrium (guided)

2.1 Maximum Entropy Estimation via Langevin Dynamics

Given a moment function $\phi : \mathbb{R}^d \rightarrow \mathbb{R}^r$ with target expectation $m \in \mathbb{R}^r$, the *maximum entropy principle* seeks the probability density function (PDF) p which satisfies the moment constraints

$$\mathbb{E}_p[\phi] = \int \phi(x)p(x) dx = m, \quad (1)$$

while maximizing the differential entropy

$$H(p) = - \int p(x) \log p(x) dx. \quad (2)$$

Since infinitely many densities satisfy the moment constraints, entropy maximization acts as a concave regularization that selects a unique solution. Introducing Lagrange multipliers $\theta \in \mathbb{R}^r$ for these constraints, the Lagrangian

$$\mathcal{L}(p, \theta) = H(p) - \theta^\top (\mathbb{E}_p[\phi] - m) \quad (3)$$

has, if a maximizer exists, a unique maximum at (p_*, θ_*) , where the maximum entropy density $p_* = p_{\theta_*}$ takes the exponential form:

$$p_\theta(x) = \mathcal{Z}_\theta^{-1} e^{-\theta^\top \phi(x)}, \quad \text{with } \mathcal{Z}_\theta = \int_{\mathbb{R}^d} e^{-\theta^\top \phi(x)} dx. \quad (4)$$

The optimal parameter θ_* equivalently maximizes $\mathcal{L}(p_\theta, \theta) = -\theta^\top m - \log \mathcal{Z}_\theta$. While direct evaluation is intractable because it requires computing the normalisation constant \mathcal{Z}_θ , the gradient can be estimated by sampling from p_θ , since

$$\nabla_\theta \mathcal{L}(p_\theta, \theta) = \mathbb{E}_{p_\theta}[\phi] - m, \quad (5)$$

because $\nabla_\theta \log \mathcal{Z}_\theta = -\mathbb{E}_{p_\theta}[\phi]$.

Sampling from p_θ is typically performed using MCMC methods [24] based e.g. on Langevin dynamics, i.e. via solution of the SDE

$$dX_t = -\sigma^2 \theta^\top \nabla \phi(X_t) dt + \sqrt{2}\sigma dW_t, \quad (6)$$

where W_t is a standard Brownian motion, σ is a volatility parameter, and ∇ denotes the gradient with respect to $x \in \mathbb{R}^d$. Under suitable conditions, the law of X_t converges to the distribution with density p_θ as $t \rightarrow \infty$ and, by ergodicity, $\mathbb{E}_{p_\theta}[\phi]$ can be estimated by a time average along the trajectory. In practice, the SDE (6) is discretized using an Euler-Maruyama scheme [25, 26], and a Metropolis-Hastings accept-reject step is added to correct for discretization bias—this is the Metropolis Adjusted Langevin Algorithm (MALA) [27].

Unfortunately, Langevin dynamics and MCMC algorithms more generally suffer from critical slowing down for non-convex energies, leading to prohibitively long equilibration times. In particular, MALA scales poorly with dimension [28, 29], with sampling time growing exponentially in most cases.

This is particularly problematic for parameter estimation, since sampling must be repeated at each iteration of the optimization over θ to update $\mathbb{E}_{p_\theta}[\phi]$ as θ changes. The computational cost of both parameter estimation and sample generation typically becomes impractical for high-dimensional distributions.

When samples $(x^i)_{i \leq n}$ of p are available, score matching [17] offers an alternative approach to the estimation of θ_* . It avoids sampling p_θ by minimizing the Fisher divergence $\mathcal{I}(p, p_\theta) = \mathbb{E}_p[|\nabla \log p_\theta - \nabla \log p|^2]$. After integration by parts, the Fisher divergence can be written, up to a constant, as an expectation over the data: $\mathcal{I}(p, p_\theta) = \mathbb{E}_p[|\nabla \log p_\theta|^2 + 2\Delta \log p_\theta] + \text{cst}$, where Δ denotes the Laplacian. The resulting score matching parameter $\tilde{\theta}_*$ that minimizes the Fisher divergence is a solution of the linear system [17]

$$\mathbb{E}_p[\nabla \phi \cdot \nabla \phi^\top] \tilde{\theta}_* = \mathbb{E}_p[\Delta \phi]. \quad (7)$$

The expectations in this equation can be estimated empirically using data samples $(x^i)_{i \leq n}$, without sampling intermediate distributions. It is therefore a much faster algorithm but $\tilde{\theta}_* = \theta_*$ only if the data distribution already belongs to the exponential family, i.e., $p = p_{\theta_*}$. This condition is usually not satisfied. Moreover, if the Gibbs energy of p is non-convex, this estimator has high variance [30], making it unreliable.

2.2 Flow Matching with Stochastic Interpolants

Since the seminal work of Ho, Song and collaborators [6, 7], complex data generation has been addressed by transporting samples between Gaussian white noise and a target distribution p , through reversal of a stochastic noising process. Transport-based generative models have since been developed under various names—flow matching [3], stochastic interpolants [4], and rectified flows [14]. These methods define time-dependent interpolations between two distributions and sample from them using flows (ODEs) or diffusions (SDEs). We adopt the stochastic interpolant formulation in what follows.

A variance preserving stochastic interpolant I_t between samples Z from a prior distribution (typically Gaussian noise, $Z \sim \mathcal{N}(0, \text{Id})$) and data $X \sim p$ is defined by

$$I_t = \cos(\alpha_t) Z + \sin(\alpha_t) X, \quad t \in [0, 1], \quad (8)$$

where α_t is a $\mathcal{C}^1([0, 1])$ function with boundary conditions $\alpha_0 = 0$ and $\alpha_1 = \frac{\pi}{2}$ (for example $\alpha_t = \frac{\pi}{2}t$), so that $I_0 = Z$ and $I_1 = X$. The key observation made in [4, 5] is that the PDF $p_t(x)$ of the interpolant I_t can be sampled via an SDE whose coefficients are estimable from data. Specifically, let X_t satisfy the SDE

$$dX_t = b_t(X_t) dt + \sigma^2 \nabla \log p_t(X_t) dt + \sqrt{2} \sigma dW_t, \quad (9)$$

where W_t is a Brownian noise and $\sigma \geq 0$ is a tunable volatility with

$$b_t(x) = \mathbb{E}[\dot{I}_t | I_t = x], \quad (10)$$

where the dot denoting the time derivative and $\mathbb{E}[\cdot | I_t = x]$ the expectation over the law of I_t conditional on $I_t = x$. Then, if $X_0 = I_0 = Z$, X_t and I_t share the same PDF p_t for all $t \in [0, 1]$. By Stein's formula, the score $\nabla \log p_t$ can also be expressed as a conditional expectation:

$$\nabla \log p_t(x) = -\frac{1}{\cos(\alpha_t)} \mathbb{E}[Z | I_t = x]. \quad (11)$$

Since a conditional expectation is the minimizer of a quadratic loss, b_t and $\nabla \log p_t$ can be learned by minimizing this loss, typically by representing them in a rich parametric class such as a deep neural network.

Unlike the Langevin SDE (6), which follows equilibrium dynamics whose law converges to p_θ only as $t \rightarrow \infty$, the SDE (9) defines a non-equilibrium transport that reaches the target distribution at time $t = 1$. Crucially, this transport avoids the critical slowing down that plagues Langevin dynamics. Because the interpolant I_t mixes data with Gaussian noise, the distribution p_t varies smoothly from a simple Gaussian at $t = 0$ to the target at $t = 1$. Particles following the SDE (9) are guided along this smooth path, with the complex structure of the target emerging gradually as $t \rightarrow 1$. For example, in multimodal distributions, particles are positioned inside the correct modes early (when the landscape is smooth) and remain there as the modes sharpen. We illustrate this in Figure 1.

Stochastic interpolants thus provide a fast sampler that approximates the data distribution. In theory, the drift b_t reproduces the full density p_t of I_t at each time, and hence the target density p at $t = 1$. With sufficient training data, deep neural networks generalize well on complex datasets [15]. It results from an implicit regularization produced by the stochastic gradient descent of the neural network optimization [31, 32], which is not well understood. In the low-data regime, however, the learned model may overfit and memorize the training samples. Maximum entropy models offer a complementary approach: they provide explicit regularization through entropy maximization, leading to analytic exponential distributions with controlled approximation error. The next section shows that they can also be sampled via stochastic interpolation.

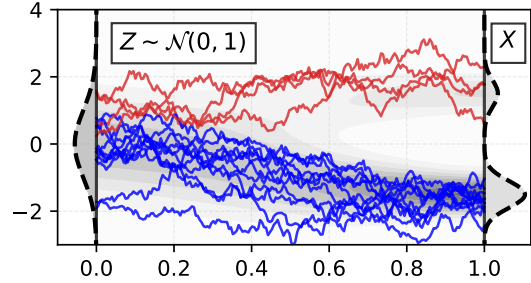


Figure 1: Illustration of trajectories (in blue or red) of X_t satisfying Equation (9) for an interpolant I_t defined with $\alpha_t = \pi t/2$ between white noise Z and a bimodal unbalanced Gaussian mixture X , for $\sigma = 1$. We display in gray in the background the density of I_t . When t goes to 0, the modes progressively disappear. At early times t , particles evolve freely in space, but they become trapped in the modes when the density p_t becomes bimodal. Red particles are confined in the upper mode and blues in the lower one.

3 Moment Guided Diffusion

In this section, we introduce Moment Guided Diffusion (MGD), which guides moments exactly along an interpolation path while injecting Langevin noise. We show that this preserves moments at each time; convergence to the maximum entropy distribution as the volatility increases will be discussed in Section 4. Section 3.1 defines the MGD SDE and establishes conditions under which it preserves moments. Section 3.2 introduces a discretized algorithm and discusses its numerical cost.

3.1 Moment Guided Diffusion

A stochastic interpolant SDE (9) produces X_t with the same distribution as I_t , thereby reproducing all moments. MGD uses the same interpolant I_t , but imposes only that a finite number of moments is preserved:

$$\forall t \in [0, 1] : \mathbb{E}[\phi(X_t)] = \mathbb{E}[\phi(I_t)] \stackrel{\text{def}}{=} m_t. \quad (12)$$

The following theorem shows that this weaker constraint is satisfied by an SDE formally similar to the Langevin equation (6), but with a time-dependent drift analogous to (10).

Theorem 3.1 (Moment Guided Diffusion). *Consider the SDE*

$$dX_t = (\eta_t^\top - \sigma^2 \theta_t^\top) \nabla \phi(X_t) dt + \sqrt{2} \sigma dW_t, \quad X_0 = Z, \quad (13)$$

where W_t is a Brownian noise and η_t and θ_t solve

$$G_t \eta_t = \frac{d}{dt} m_t, \quad (14)$$

$$G_t \theta_t = \mathbb{E}[\Delta \phi(X_t)], \quad (15)$$

where G_t is the Gram matrix

$$G_t = \mathbb{E}[\nabla \phi(X_t) \cdot \nabla \phi(X_t)^\top]. \quad (16)$$

If this coupled system admits a solution, then the moment condition $\mathbb{E}[\phi(X_t)] = m_t$ holds for all $t \in [0, 1]$.

The proof of Theorem 3.1 is given in Appendix A. By applying Itô's lemma, we show that any solution satisfies

$$\forall t \in [0, 1] : \frac{d}{dt} \mathbb{E}[\phi(X_t)] = \frac{d}{dt} m_t, \quad (17)$$

which implies $\mathbb{E}[\phi(X_t)] = m_t$ since this holds at $t = 0$.

Note that the existence of a solution needs to be assumed. Since G_t , η_t , and θ_t depend on the law of X_t , (13) is a nonlinear (McKean–Vlasov) SDE [33, 34] whose well-posedness is non-trivial. In particular, G_t may become singular, causing the drift to blow up. Sufficient conditions for existence are established in Appendix F: Theorem F.7 proves that for large enough σ , a version of MGD with an additional confining potential admits strong solutions X_t that converge to the maximum entropy distribution with moments m_t . The proof relies on the assumption that the Poincaré constant of a reference measure is finite.

If p_0 is Gaussian and $\phi(x) = (x, xx^\top)$, then MGD solutions exist and are independent of σ . In particular, one may set $\sigma = 0$, reducing the SDE (13) to an ODE. Appendix E shows that under these hypotheses, X_t is Gaussian with the same mean and covariance as I_t , so MGD exactly samples the maximum entropy distribution for all $\sigma \geq 0$.

Remark 3.2 (Sampling vs. modelling error). *Throughout this paper, “exact sampling” refers to sampling from the maximum entropy distribution p_* constrained by $\mathbb{E}_{p_*}[\phi] = \mathbb{E}[\phi(X)]$, not from the true data distribution p . The discrepancy $D_{\text{KL}}(p\|p_*)$ reflects model misspecification inherent to the choice of moment function ϕ , and is distinct from the sampling error $D_{\text{KL}}(p_1^\sigma\|p_*)$ that MGD controls (if p_1^σ is the density of X_1).*

For general ϕ , the dynamics at $\sigma = 0$ typically does not yield the distribution of X_1 to be the maximum entropy distribution with moments $\mathbb{E}[\phi(X)]$. The volatility σ controls convergence to maximum entropy: Brownian noise increases entropy, while the guidance η_t can reduce it. When σ is large, the noise dominates. We conjecture (Section 4) and verify numerically (Section 5) that $p_1^\sigma \rightarrow p_$ as $\sigma \rightarrow \infty$. It means that MGD eliminates the sampling error while the modelling error remains a choice dictated by ϕ .*

Turning now to the structure of the MGD SDE, the drift in (13) has two components: η_t steers the process to adjust the target moments m_t to m_{t+dt} , while $\sigma^2 \theta_t$ counterbalances the moment modification induced by the added white noise σdW_t . Note that the MGD SDE (13) is structurally similar to the stochastic interpolant SDE (9): it has a transport term proportional to η_t (analogous to b_t) and a score-like term proportional to θ_t (analogous to $\nabla \log p_t$). In particular, θ_t solves an equation of the same form as the score matching equation (7), but with expectations taken over the law of X_t rather than the data distribution p .

As with stochastic interpolants (Section 2.2), MGD defines a non-equilibrium homotopic transport that reaches the target moments at $t = 1$, see Section 4.1 for more discussion. We stress, however, that $\theta_t^\top \nabla \phi(x)$ is not the score of the PDF of X_t . Unlike the stochastic interpolant SDE, where the score term is exact, the MGD drift does not reproduce the full distribution of I_t but only its moments $\mathbb{E}[\phi(I_t)]$. This is the key difference between MGD and stochastic interpolants.

Remark 3.3. *Observe that θ_1 in (15) coincides with the score matching parameter in (7) computed for X_1 . If the distribution of X_1 converges to p_* as $\sigma \rightarrow \infty$, then θ_1 converges to θ_* . A finite sample estimator of θ_1 is thus a nearly consistent estimator of θ_* for large σ . However, as noted in Section 2, score matching estimators have high variance for non-convex energies. Crucially, MGD’s sampling accuracy depends on the empirical estimation of m_t , not on the accuracy of θ_t (see Section 5.2.)*

3.2 Discretization of MGD

We solve numerically the MGD nonlinear (McKean–Vlasov) SDE (13) by iteratively updating a finite ensemble of interacting particles. To update the particles, we estimate η_t in (14) and θ_t in (15) with empirical means over these particles. We also avoid computing $\mathbb{E}[\Delta\phi]$, which is costly or ill-defined when ϕ is not smooth. This is achieved with a two-step predictor-corrector scheme, which we first describe using exact expectations before discussing finite-particle estimations.

Given X_t and some small time step $h > 0$, let Y be obtained via

$$Y = X_t + h \eta_t^\top \nabla \phi(X_t) + \sqrt{2}\sigma(W_{t+h} - W_t), \quad (18)$$

with η_t the solution to (14). This is the Euler–Maruyama scheme for the MGD SDE (13) with $\theta_t = 0$. As such, the update (18) does not preserve the moments, i.e. $\mathbb{E}[\phi(Y)] \neq m_{t+h}$. We enforce this moment condition by adding to Y a term similar to the one involving θ_t in the MGD SDE (13), i.e. setting

$$X_{t+h} = Y - h \sigma^2 \hat{\theta}^\top \nabla \phi(Y), \quad (19)$$

and requiring that

$$\mathbb{E}[\phi(X_{t+h})] = m_{t+h}. \quad (20)$$

Substituting (19) into (20) gives an equation for $\hat{\theta}$. Solving this exactly is costly (it is nonlinear in $\hat{\theta}$) and unnecessary, since the Euler–Maruyama update is only accurate to weak order 1 in h . Working to the same order of accuracy, we Taylor expand the left-hand side of (20) to obtain

$$h \sigma^2 \mathbb{E}[\nabla \phi(Y) \cdot \nabla \phi(Y)^\top] \hat{\theta} = \mathbb{E}[\phi(Y)] - m_{t+h}. \quad (21)$$

Since $\mathbb{E}[\phi(X_t)] = m_t$, the right-hand side equals $h \mathbb{E}[\Delta\phi(X_t)] + o(h)$, so to leading order (21) reduces to (15) and $\hat{\theta} = \theta_t$. In the numerical scheme, however, it is more convenient to solve (21) directly since this avoids computing $\mathbb{E}[\Delta\phi(X_t)]$. This is important when ϕ includes ℓ^1 norms or absolute values, for which $\Delta\phi$ is a

sum of Dirac functions whose expectation is hard to estimate unless the number of samples is very large.

To turn this into a practical scheme, we need to choose the time step h . Since the drift is proportional to σ^2 for large σ , so is its Lipschitz constant. We therefore set the number of steps to $n_\sigma = a\sigma^2 + b$, where b ensures the limiting ODE ($\sigma \rightarrow 0$) is accurately solved. The computational cost of MGD thus scales as $O(\sigma^2)$.

The scheme is summarized in Algorithm 1. It iteratively evolves a population of n_{rep} particles $(x_k^i)_{1 \leq i \leq n_{\text{rep}}}$ (replicas), whose empirical measure approximates the distribution of X_{k/n_σ} , using moments m_t estimated from training data. A key property is that the moment condition (20) remains valid when expectations are replaced by empirical averages over particles, since (21) holds for empirical distributions. As a result, the empirical mean of ϕ over the particles converges to m_{t+h} as the step size $h \rightarrow 0$. This exact moment tracking controls the dynamical stability of the algorithm: a divergence of particles would manifest as a moment mismatch (see Remark 3.3). Alternative implementations are discussed Appendix C and some numerical details in Appendix D.

Algorithm 1 Moment-Guided Diffusion (MGD)

Input: volatility σ ; number of steps $n_\sigma = O(\sigma^2)$; time step $h = 1/n_\sigma$; number of replicas n_{rep} ; moments $m_t = \mathbb{E}[\phi(I_t)]$
Initialize: $x_0^i \sim \mathcal{N}(0, \text{Id})$ for $i = 1, \dots, n_{\text{rep}}$
Predictor
for $k = 0, \dots, n_\sigma - 1$ **do**
 Compute $\hat{G}_k = \frac{1}{n_{\text{rep}}} \sum_{i=1}^{n_{\text{rep}}} \nabla \phi(x_k^i) \cdot \nabla \phi(x_k^i)^\top$
 Solve $\hat{G}_k \hat{\eta}_k = \frac{d}{dt} m_{kh}$ for $\hat{\eta}_k$
 for $i = 1, \dots, n_{\text{rep}}$ **do**
 Sample $\xi_k^i \sim \mathcal{N}(0, \text{Id})$
 Set $y_k^i = x_k^i + h \hat{\eta}_k^\top \nabla \phi(x_k^i) + \sqrt{2h}\sigma \xi_k^i$
 end for
 Corrector (project to preserve moments)
 Compute $\hat{G}'_k = \frac{1}{n_{\text{rep}}} \sum_{i=1}^{n_{\text{rep}}} \nabla \phi(y_k^i) \cdot \nabla \phi(y_k^i)^\top$
 Solve $h\sigma^2 \hat{G}'_k \hat{\theta}_k = \frac{1}{n_{\text{rep}}} \sum_{i=1}^{n_{\text{rep}}} \phi(y_k^i) - m_{(k+1)h}$ for $\hat{\theta}_k$
 for $i = 1, \dots, n_{\text{rep}}$ **do**
 Set $x_{k+1}^i = y_k^i + h \hat{\theta}_k^\top \nabla \phi(y_k^i)$
 end for
end for
Output: Samples $(x_{n_\sigma}^i)_{1 \leq i \leq n_{\text{rep}}}$

4 Maximum Entropy: Convergence and Bounds

Let p_t^σ be the PDF of the solution X_t of the MGD SDE (13) for a volatility σ . Section 4.1 studies the convergence of p_1^σ towards the maximum entropy distribution p_* . Section 4.2 computes a tractable lower bound of the

entropy $H(p_1^\sigma)$ and conjectures its convergence towards $H(p_*)$ when σ increases.

4.1 Convergence towards the Maximum Entropy Distribution

A central claim of this paper is that, as $\sigma \rightarrow \infty$, the distribution p_1^σ of the MGD output converges to the maximum entropy distribution p_* . Next, we provide heuristic support for this claim via a formal Taylor expansion, then state it precisely as Conjecture 4.1. The conjecture is verified numerically in Section 5.

The time evolution of the PDF p_t^σ of the solution of the MGD SDE (13) is governed by the Fokker-Planck equation:

$$\partial_t p_t^\sigma = \nabla \cdot (p_t^\sigma ((-\eta_t + \sigma^2 \theta_t)^\top \nabla \phi)) + \sigma^2 \Delta p_t^\sigma. \quad (22)$$

Formally taking $\sigma \rightarrow \infty$ and keeping only the leading-order terms, the Fokker-Planck equation reduces to

$$\nabla \cdot (p_t^* (\theta_t^* \top \nabla \phi)) + \Delta p_t^* = 0, \quad (23)$$

where p_t^* and θ_t^* denote the (formal) limits of p_t^σ and θ_t as $\sigma \rightarrow \infty$. The solution of this limit equation is an exponential distribution:

$$p_t^* = (\mathcal{Z}_t^*)^{-1} e^{-\theta_t^* \top \phi}, \quad (24)$$

with normalising constant \mathcal{Z}_t^* . This suggests that p_t^σ converges to an exponential distribution with moments m_t , and hence to the maximum entropy distribution satisfying these constraints. In particular, this gives $p_1^* = p_*$ and $\theta_1^* = \theta_*$. Expanding $p_t^\sigma = p_t^*(1 + q_t \sigma^{-2} + o(\sigma^{-2}))$, for some q_t that does not depend upon σ , Appendix B provides a formal calculation showing that the Kullback-Leibler divergence satisfies $D_{\text{KL}}(p_1^\sigma \| p_*) = O(\sigma^{-2})$. This leads to the following conjecture:

Conjecture 4.1 (Max entropy). *There exists $C > 0$ such that for all $\sigma > 0$*

$$D_{\text{KL}}(p_1^\sigma \| p_*) \leq C \sigma^{-2}. \quad (25)$$

A numerical verification is given in Section 5. Since p_1^σ and p_* share the same moments, we have

$$D_{\text{KL}}(p_1^\sigma \| p_*) = H(p_*) - H(p_1^\sigma), \quad (26)$$

so (25) is equivalent to

$$H(p_*) - H(p_1^\sigma) \leq C \sigma^{-2}. \quad (27)$$

Remark 4.2. *In numerical experiments, we choose p_0 to be a Gaussian PDF. If ϕ is quadratic ($\phi(x) = xx^\top$) since $\nabla \phi(x)$ is linear, dX_t in the MGD (22) is the sum of two Gaussian random vectors so X_t remains Gaussian for all t with second order moments equal to m_t . It results that p_t^σ is Gaussian with the same mean and covariance as I_t , and does not depend on σ . More generally, Theorem E.1 in Appendix E proves that for any sufficiently regular p_0 , if $\phi(x) = (x, xx^\top)$, then MGD admits strong solutions and*

$$\lim_{\sigma \rightarrow \infty} D_{\text{KL}}(p_1^\sigma \| p_*) = 0.$$

Since the numerical cost of MGD is $O(\sigma^2)$ (see Section 3.2), the cost required to reach a given error is proportional to the constant C appearing in Conjecture 4.1. This constant depends on the moment function ϕ and the moments m_t , and becomes large when ϕ is not expressive enough to capture the homotopic transport of mass at early times t —before the maximum entropy distribution with moments m_t becomes multimodal.

If $x \in \mathbb{R}$, a truncated monomial basis $\phi(x) = (x^k)_{k \leq r}$ provides this flexibility, as illustrated in Section 5.1. If $x \in \mathbb{R}^d$, since the number of monomials grows polynomially with d , this strategy becomes computationally prohibitive for d large. A wavelet scattering spectra ϕ [21] computes $O(\log^3 d)$ low-order multiscale moments that are similar to fourth order moments. In Section 6, we show that for real-world high-dimensional datasets from physics and finance, it is sufficient rich to capture this homotopic transport with a small C .

Modelling the transport of mass does not require ϕ to provide an accurate model the full distribution of I_t . We show in Section 6.5 that C can be small although the model misspecification $D_{\text{KL}}(p\|p_*)$ is large.

4.2 Entropy Estimation

We now compute a tractable lower bound on the entropy $H(p_1^\sigma)$ and conjecture that it converges to $H(p_*)$ as $\sigma \rightarrow \infty$.

Proposition 4.3. *Assume the MGD SDE (13) admits a unique strong solution for all $t \in [0, 1]$. Then,*

$$\begin{aligned} \frac{d}{dt} H(p_t^\sigma) &= \theta_t^\top \frac{d}{dt} m_t \\ &+ \sigma^2 \mathbb{E}[|\nabla \log p_t^\sigma(X_t) + \theta_t^\top \nabla \phi(X_t)|^2], \end{aligned} \quad (28)$$

and hence

$$\frac{d}{dt} H(p_t^\sigma) \geq \theta_t^\top \frac{d}{dt} m_t. \quad (29)$$

The proof, given in Appendix A, uses the Fokker-Planck equation (22) to compute the evolution of the differential entropy of p_t^σ . When the moments are constant ($\frac{d}{dt} m_t = 0$), the entropy increases along the dynamics. In this case, $H(p_t^\sigma)$ also increases with σ , as shown by a time-rescaling argument in Proposition A.1. Sections 5 and 6 provide numerical verification that $\frac{d}{d\sigma} H(p_t^\sigma) \geq 0$ more generally.

Integrating (29) over $[0, 1]$ yields a lower bound on the entropy of the sampled distribution p_1^σ :

$$H(p_1^\sigma) \geq H_*^\sigma := H(p_0) + \int_0^1 \theta_t^\top \frac{d}{dt} m_t dt. \quad (30)$$

This lower bound can be computed directly from the MGD parameters along the dynamics. From (28), the gap between $H(p_1^\sigma)$ and its lower bound is

$$H(p_1^\sigma) - H_*^\sigma = \sigma^2 \int_0^1 \mathbb{E}[|\nabla \log p_t^\sigma(X_t) + \theta_t^\top \nabla \phi(X_t)|^2] dt. \quad (31)$$

This integral is the time-averaged Fisher divergence between p_t^σ and the exponential distribution with energy $\theta_t^\top \phi$. If Conjecture 4.1 holds, this Fisher divergence vanishes as $\sigma \rightarrow \infty$, provided that p_0 itself has an exponential form. In particular, this holds when $X_0 = Z$ is Gaussian and ϕ includes quadratic terms so that $\theta_0^\top \phi(x) = |x|^2/2$ for some θ_0 . The lower bound H_*^σ then converges towards $H(p_*)$.

Conjecture 4.4 (Entropy bound). *If Z has density $p_0 = Z_0^{-1} e^{-\theta_0^\top \phi}$, then there exists $C > 0$ such that for all $\sigma > 0$,*

$$H(p_*) - H_*^\sigma \leq C \sigma^{-2}. \quad (32)$$

Supporting arguments from the same Fokker-Planck analysis are given in Appendix B, with numerical verification in Section 5. In practice, monitoring the convergence of H_*^σ provides a diagnostic for the convergence of p_1^σ to p_* .

5 Numerical Validation

Section 5.1 studies the numerical convergence properties of Moment Guided Diffusions towards maximum entropy distributions, over distributions of one-dimensional $x \in \mathbb{R}$. We use a cosine interpolant defined by

$$I_t = \cos(\frac{1}{2}\pi t) Z + \sin(\frac{1}{2}\pi t) X$$

and solve the MGD SDE (13) with the numerical integrator specified in Section 3.2. Section 5.2 shows empirically that the numerical complexity of the MGD sampling does not suffer from the non-convexity of the distributions as opposed to an MCMC sampling algorithm.

5.1 Convergence towards Maximum Entropy Distributions

The MGD algorithm samples a distribution with density p_1^σ . We study its numerical convergence to the maximum entropy distribution $p_*(x) = Z_{\theta_*}^{-1} e^{-\theta_*^\top \phi(x)}$ and verify Conjectures 4.1 and 4.4 for different choices of data distributions and moment functions ϕ .

5.1.1 Non-log-concave Density

We consider data $X \sim p$ distributed according to an unbalanced bimodal density $p(x) = Z^{-1} e^{-\frac{4}{5}(x^4 - 5x^2 - x/2)}$ for $x \in \mathbb{R}$, and the four-dimensional monomial map $\phi(x) = (x, x^2, x^3, x^4)$, whose moments are $\mathbb{E}[\phi(X)] \approx (0.8, 2.4, 2.2, 6.4)$. With this choice, the maximum entropy density satisfies $p_*(x) = p(x)$. (Note that I_t for $t \in (0, 1)$ is not distributed according to the maximum entropy distribution with moments m_t .)

The log-density $\log p_*(x)$ (dotted line) in Figure 2(a) exhibits two modes, reflecting a non-convex Gibbs energy. For small σ , the density p_1^σ concentrates in two separate modes. Although these modes do not have the correct shape (they are too peaked, reflecting the lack of entropy of p_1^σ), their relative weight is correct. As σ increases, the added noise allows particles to spread correctly inside the

modes, and p_1^σ progressively converges towards p_* , with near-superposition at $\sigma^2 = 5$.

Figure 2(b) quantifies this convergence via the entropy $H(p_1^\sigma)$ (blue), computed numerically from the distributions above. These values lie below $H(p_*) = 0.67$ (red). We observe that $\frac{d}{d\sigma} H(p_1^\sigma) \geq 0$ and that $H(p_1^\sigma) \rightarrow H(p_*)$ as σ^2 increases. Figure 2(c) shows $D_{\text{KL}}(p_1^\sigma \| p_*) = H(p_*) - H(p_1^\sigma)$ (blue dots), which decays as $O(\sigma^{-2})$ on the log-log scale (black dashed line shows σ^{-2} decay), validating Conjecture 4.1.

The lower bound H_*^σ on $H(p_1^\sigma)$, computed from (30), is shown as black dots in Figure 2(b). As expected, it lies below $H(p_1^\sigma)$ (blue) and also converges to $H(p_*)$. Figure 2(c) shows that $H(p_*) - H_*^\sigma$ (black dots) also decays as $O(\sigma^{-2})$, validating Conjecture 4.4.

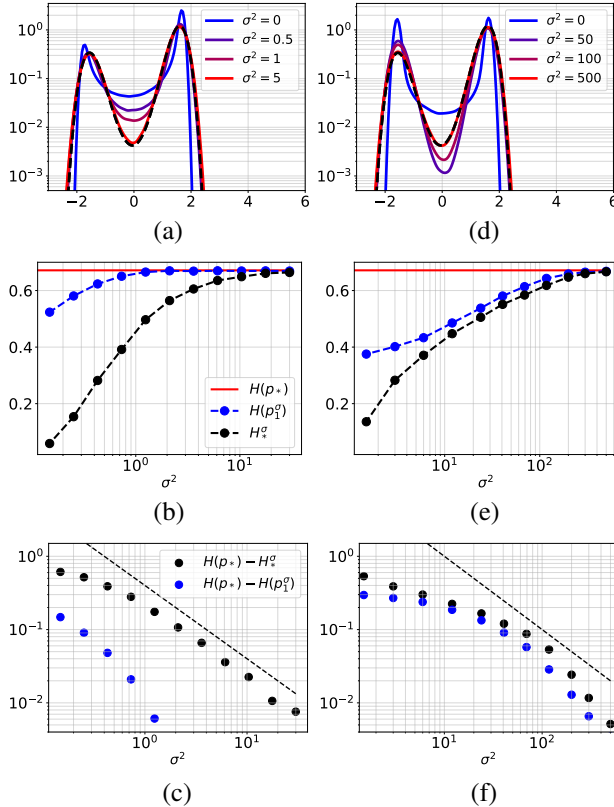


Figure 2: Convergence of MGD towards the maximum entropy bimodal distribution $p_*(x) = \mathcal{Z}^{-1} e^{-\frac{4}{5}(x^4 - 5x^2 - x/2)}$ for $X \sim p = p_*$. Left column: moment function $\phi(x) = (x, x^2, x^3, x^4)$. Right column: $\phi(x) = (x^2, \log p(x))$. (a,d) Log-density $\log p_*(x)$ (dashed) and $\log p_1^\sigma(x)$ for increasing σ (blue to red). (b,e) Maximum entropy $H(p_*)$ (red line), sampled entropy $H(p_1^\sigma)$ (blue dots), and lower bound H_*^σ from (30) (black dots) versus σ^2 . (c,f) Entropy gaps $H(p_*) - H(p_1^\sigma)$ (blue) and $H(p_*) - H_*^\sigma$ (black) versus σ^2 ; the dashed line shows σ^{-2} decay.

5.1.2 Slower Convergence

In the previous example, p_1^σ converges towards p_* with negligible error for $\sigma^2 \geq 2$. We now show that the convergence constant C in Conjecture 4.1 depends critically on the choice of moment functions ϕ .

When p is known, a seemingly natural choice is $\phi(x) = (x^2, \log p(x))$, since this suffices to represent both the data density p and the initial Gaussian density p_0 , yielding $p_*(x) = p(x)$. For the bimodal density $p(x) = \mathcal{Z}^{-1} e^{-\frac{4}{5}(x^4 - 5x^2 - x/2)}$ with this ϕ , Figures 2(e) and (f) confirm that $D_{\text{KL}}(p_1^\sigma \| p_*)$ and $H(p_*) - H_*^\sigma$ both decay as $C\sigma^{-2}$ for $\sigma^2 \geq 50$, validating Conjectures 4.1 and 4.4. However, the constant C is much larger than in the previous example: small errors require $\sigma^2 \geq 500$, or approximately 10^2 times more integration steps.

Figure 2(d) shows the densities p_1^σ for several values of σ . Although p_1^σ is bimodal for $\sigma^2 \leq 1$, the relative weights of the two modes are off by one order of magnitude. This occurs because ϕ is not expressive enough to displace mass at early times t of the MGD, before p_t^σ becomes multimodal. For larger values of σ^2 (above 10^2), MGD becomes analogous to a Langevin dynamic, recovering the correct relative weights through random switching of particles between modes.

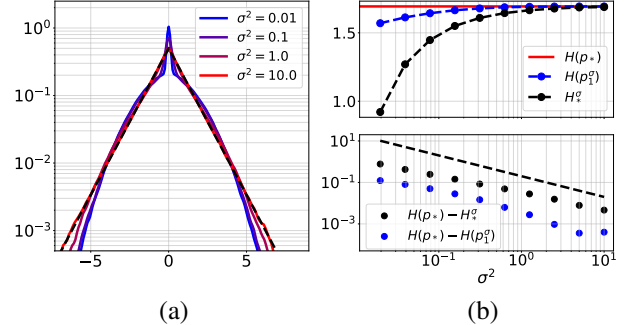


Figure 3: Convergence of MGD towards the Laplacian maximum entropy distribution $p_*(x) = \frac{1}{2} e^{-|x|}$ for $X \sim p = p_*$. (a) Log-density $\log p_*(x)$ (dashed) and $\log p_1^\sigma(x)$ for increasing σ (blue to red). (b, top) Maximum entropy $H(p_*)$ (red line), sampled entropy $H(p_1^\sigma)$ (blue dots), and lower bound H_*^σ from (30) (black dots) versus σ^2 . (b, bottom) Entropy gaps $H(p_*) - H(p_1^\sigma)$ (blue) and $H(p_*) - H_*^\sigma$ (black) versus σ^2 ; the dashed line shows σ^{-2} decay.

5.1.3 Non-smooth ϕ

The MGD numerical scheme (Section 3.2) avoids computing $\Delta\phi$, which is essential when ϕ includes modulus or ℓ_1 norms, as in the scattering spectra of Section 6. We verify here that MGD correctly samples maximum entropy distributions defined by non-smooth ϕ , and that Conjectures 4.1 and 4.4 hold.

We consider data distributed according to the Laplacian density $p(x) = \frac{1}{2} e^{-|x|}$, which is the maximum entropy

distribution $p = p_*$ for $\phi(x) = (x^2, |x|)$ with $\mathbb{E}[\phi(X)] = (2, 1)$. Figure 3(a) shows $\log p_1^\sigma(x)$ for various σ . As σ increases, the curves converge to $\log p_*(x)$ (dashed), nearly superimposing at $\sigma^2 = 10$. For small σ , the density p_1^σ exhibits a sharper spike near zero and shorter tails, reflecting insufficient entropy.

Convergence is quantified by $D_{\text{KL}}(p_1^\sigma \| p_*) = H(p_*) - H(p_1^\sigma)$, which decreases to zero as σ^2 increases (Figure 3(b, top)). Figure 3(b, bottom) confirms $H(p_*) - H(p_1^\sigma) = O(\sigma^{-2})$ for $\sigma^2 \geq 10^{-2}$, validating Conjecture 4.1. The lower bound H_*^σ from (30) (black dots) also converges to $H(p_*)$ at the same rate, validating Conjecture 4.4. Since the Laplacian is log-concave: there is no mass to displace between wells, so even a Langevin dynamic would converge quickly.

5.2 Rate of Convergence and Multimodality

We verify numerically that the computational cost of MGD does not depend on energy barrier heights, unlike MCMC methods. We use truncated monomial moment generating functions $\phi(x) = (x^k)_{k \leq r}$ (for $r = 4$)

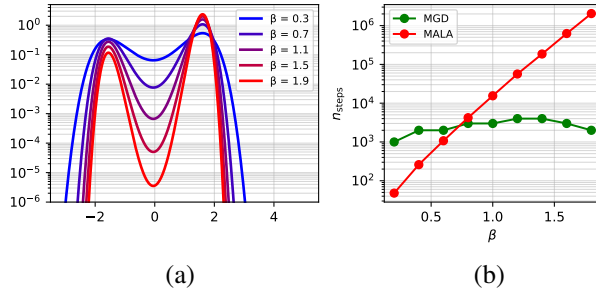


Figure 4: (a) Log-density $\log p_*(x)$ for $p_*(x) = Z_\beta^{-1} e^{-\beta(x^4 - 5x^2 - x/2)}$ with increasing β (blue to red). The two modes are separated by a barrier of height proportional to β . (b) Number of discretization steps n_{steps} required to reach a fixed Kullback–Leibler divergence from p_* , for MALA (red) and MGD (green), as a function of β . For MALA, n_{steps} grows exponentially with β ; for MGD, it remains nearly constant.

Figure 4(a) shows the log-density of unbalanced bimodal distributions

$$p_*(x) = Z_\beta^{-1} e^{-\beta(x^4 - 5x^2 - x/2)},$$

with two modes separated by a barrier of height proportional to β . For MGD, we consider for simplicity that X is distributed according to the maximum entropy distribution $p = p_*$. The computational cost of both MGD and the Metropolis Adjusted Langevin Algorithm (MALA) is proportional to the number n_{steps} of discretization steps. The cost per step differs between algorithms (typically higher for MGD), but it does not depend on β so we do take it into account.

MALA computes samples via discretized Langevin dynamics initialized from Gaussian white noise, with an

accept-reject operation which eliminates the discretization bias. The step size is tuned to achieve an optimal acceptance rate approximately 0.57 [35]. Although the sampled distribution \tilde{p} converges to p_* as n_{steps} increases, this convergence depends exponentially on β . Indeed, crossing an energy barrier by adding Gaussian noise has probability exponentially small in the barrier height.

We measure the minimum number of steps n_{steps} required to reach a fixed error $D_{\text{KL}}(\tilde{p} \| p_*) = 10^{-3}$. Figure 4(b) confirms that for MALA (red), n_{steps} grows exponentially with β , making it computationally prohibitive for non-convex distributions—especially in higher dimensions.

For MGD, we know that $n_{\text{steps}} = n_\sigma = O(\sigma^2)$ and $D_{\text{KL}}(p_1^\sigma \| p_*) = O(\sigma^{-2})$. We choose σ so that the discretized MGD satisfies $D_{\text{KL}}(\tilde{p}_1^\sigma \| p_*) = 10^{-3}$. We run this experiment for the moment generating function $\phi(x) = (x, x^2, x^3, x^4)$. Figure 4(b) shows that for MGD (green), n_{steps} remains approximately constant as β increases. It verifies that the MGD computational cost does not suffer from multimodality.

The homotopic transport (Section 4.1) is able to distribute samples into correct modes early, enabling efficient sampling. However, this property requires ϕ to be sufficient rich to capture the mass transport at early times; for $\phi(x) = (x^2, \log p(x))$, MGD would revert to MCMC-like behavior.

6 Generation of Multiscale Processes in Finance and Physics

This section applies the MGD algorithm to sample high-dimensional maximum entropy distributions. Section 6.2 reviews multiscale maximum entropy models based on wavelet scattering moments. We consider financial time series (Section 6.3) as well as two-dimensional turbulent and cosmological fields (Section 6.2). To validate Conjectures 4.1 and 4.4, we compute the lower bound of the entropy of sampled distributions, and study its convergence as the volatility σ increases. We also estimate negentropy, which quantifies order and non-Gaussianity (Section 6.1). Finally, we show numerically in Section 6.5 that the convergence of MGD to the maximum entropy distribution p_* does not depend upon the model error $D_{\text{KL}}(p \| p_*)$.

6.1 Negentropy Rate

The negentropy was introduced in statistical physics by Erwin Schrödinger [16] to measure the distance of system to equilibrium, and give a measure of order and information. The negentropy usually can not be measured for high-dimensional systems because estimating the entropy is generally untractable.

The negentropy of a random vector X is defined as the difference between the entropy $H(p)$ of the density p of X and the entropy $H(g)$ of the gaussian density g having the same covariance Σ as p . The negentropy rate is

normalised by the dimension d of X and can be rewritten as the Kullback Leibler divergence between p and the Gaussian g :

$$\Delta H(p) = d^{-1}(H(g) - H(p)) = d^{-1}D_{\text{KL}}(p\|g) \geq 0, \quad (33)$$

where the Gaussian entropy is given by

$$H(g) = \frac{d}{2} \log \left(2\pi e (\det \Sigma)^{1/d} \right). \quad (34)$$

The negentropy rate converges when d goes to infinity for extensive processes for which the entropy rate $d^{-1}H(p)$ converges. It is invariant to the action of an invertible linear operator on X and hence does not depend upon the covariance of X , if it is invertible. In that sense it is an intrinsic measure of non-Gaussian properties of X .

If p_* is the maximum entropy distribution conditioned by the moment value $\mathbb{E}_p(\phi)$ then $H(p_*) \geq H(p)$ and $H(p_*) - H(p) = D_{\text{KL}}(p\|p_*)$ and, as a result,

$$\Delta H(p) = d^{-1}(H(g) - H(p_*) + D_{\text{KL}}(p\|p_*)). \quad (35)$$

This implies that $d^{-1}(H(g) - H(p_*))$ is a lower bound of the negentropy $\Delta H(p)$ of p , which depends upon the accuracy of the maximum entropy model p_* defined by $D_{\text{KL}}(p\|p_*)$. The following sections give an estimate of this negentropy rate with the MGD algorithm, by computing the lower bound H_*^σ in (30) of $H(p_*)$, and

$$\Delta H_*^\sigma = d^{-1}(H(g) - H_*^\sigma). \quad (36)$$

The convergence of H_*^σ when σ increases is equivalent to the convergence of ΔH_*^σ . In particular, Conjecture 4.4 states that ΔH_*^σ should converge at rate $O(\sigma^{-2})$.

6.2 Wavelet Scattering Spectra

The wavelet scattering transform was introduced in [36] for signal classification and modelling. We compute maximum entropy models from wavelet scattering moments [19, 21]. These moments capture dependencies across scales using a complex wavelet transform. Until now, such high-dimensional maximum entropy distributions could only be sampled with a microcanonical gradient descent algorithm [18], which introduces approximation errors. We briefly review complex wavelet transforms in one and two dimensions before defining wavelet scattering moments.

6.2.1 Wavelet Transform

A wavelet $\psi(u)$ is a function with fast decay in $u \in \mathbb{R}^\kappa$ satisfying $\int \psi(u) du = 0$. Its Fourier transform is centred at a frequency $\xi \neq 0$ with fast decay away from ξ . Here $\kappa = 1$ for time series and $\kappa = 2$ for images. In numerical applications we use a *Morlet* wavelet

$$\psi(u) = \frac{1}{(2\pi\sigma^2)^{\kappa/2}} e^{-\frac{|u|^2}{2\sigma^2}} \left(e^{i\xi^\top u} - c \right),$$

where c is adjusted so that $\int \psi(u) du = 0$. As in [19, 21], we set $\sigma = 0.8$, and $\xi = 3/4$ if $\kappa = 1$ and $\xi = (3/4, 0)$ if

$\kappa = 2$. Figure 5(a,b) shows the real and imaginary parts of ψ in one and two dimensions.

In one dimension, wavelets are dilated by a scale 2^j :

$$\psi_\lambda(u) = 2^{-j/2} \psi(2^{-j}u).$$

The Fourier transform of ψ_λ is centred at frequency $\lambda = 2^{-j}\xi$. In two dimensions, the wavelet is also rotated by an angle $\ell\pi/L$ for $0 \leq \ell < L$:

$$\psi_\lambda(u) = 2^{-j\kappa/2} \psi(2^{-j}R_\ell u), \quad (37)$$

with centre frequency $\lambda = 2^{-j}R_\ell\xi$. We use $L = 4$ orientations in all experiments.

The wavelet transform of X is an invertible linear operator which captures variations at all scales 2^j and orientations $\ell\pi/L$, equivalently filtering into frequency bands of constant octave bandwidth centred at each λ [37]. It is computed via discrete convolutions on the sampling grid of X of size d , with periodic boundary conditions:

$$X^\lambda(u) := \underset{\text{def}}{X * \psi_\lambda(u)}. \quad (38)$$

The scale 2^j satisfies $1 < 2^j \leq d$, so there are at most $\log_2 d$ wavelet frequencies λ in one dimension, and at most $L \log_2 d$ in two dimensions. The lowest frequencies are captured by a low-pass filter ψ_0 centred at $\lambda = 0$.

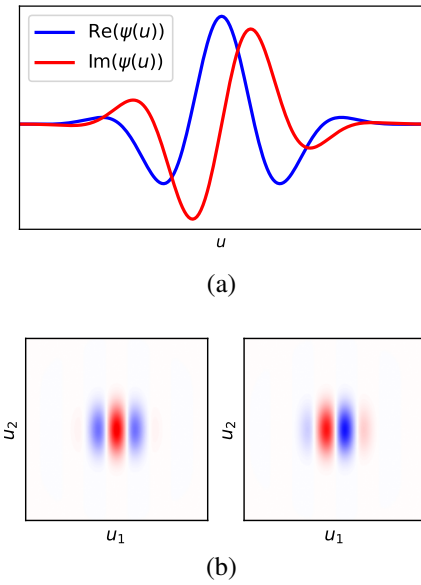


Figure 5: (a): One-dimensional Morlet wavelet ψ . The wavelet is a complex function whose real and imaginary parts are respectively in blue and red. (b): real (left) and imaginary (right) parts of a two-dimensional Morlet wavelet.

6.2.2 Wavelet Scattering Spectra

The wavelet scattering transform was introduced in [36] for signal classification and modelling. We summarize the

calculation of empirical wavelet scattering moments used in the numerical experiments of Sections 6.3 and 6.4.

The modulus of complex wavelet coefficients $|X^\lambda|$ measures the amplitude of local signal variations at multiple scales and orientations. The first two empirical scattering moments are empirical means of $|X^\lambda(u)|$ and $|X^\lambda(u)|^2$:

$$\begin{aligned}\phi_1(X) &= \left(d^{-1} \sum_u |X^\lambda(u)| \right)_\lambda, \\ \phi_2(X) &= \left(d^{-1} \sum_u |X^\lambda(u)|^2 \right)_\lambda.\end{aligned}\quad (39)$$

These empirical averages converge to expected values as d increases, under appropriate ergodicity assumptions. The dimension of ϕ_1 and ϕ_2 is $O(\log d)$. The ratio $\sum_u |X^\lambda(u)| / \sum_u |X^\lambda(u)|^2$ decreases when the sparsity of X^λ increases.

Interactions across scales are captured by a second wavelet transform of each modulus, $|X^\lambda| * \psi_{\lambda'}$, which measures variations of $|X^\lambda(u)|$ at lower frequencies $|\lambda'| < |\lambda|$. We get $O(\log_2^2 d)$ cross-scale correlations with wavelet coefficients $X^{\lambda'}$ at the frequency λ'

$$\phi_3(X) = \left(d^{-1} \sum_u |X^\lambda| * \psi_{\lambda'}(u) X^{\lambda'}(u)^* \right)_{\lambda', \lambda}, \quad (40)$$

for all λ, λ' with $|\lambda| > |\lambda'|$. The imaginary parts of these moments are sensitive to the transformation $X(u) \rightarrow X(-u)$, allowing them to characterize temporal asymmetries for 1D signals and spatial asymmetries for 2D fields.

We also compute $O(\log_2^3 d)$ cross-scale correlations between modulus wavelet coefficients at different frequencies λ and λ'' , filtered by a same wavelet of frequency λ'

$$\phi_4(X) = \left(d^{-1} \sum_u |X^\lambda| * \psi_{\lambda'}(u) |X^{\lambda''}| * \psi_{\lambda'}(u)^* \right)_{\lambda, \lambda', \lambda''}, \quad (41)$$

for all $|\lambda| > |\lambda'|$ and $|\lambda''| > |\lambda'|$. Observe that if we replace $|X^\lambda|$ by $|X^\lambda|^2$ then $\phi^3(X)$ and $\phi^4(X)$ are empirical moments of order 3 and 4. As explained in [19, 21], using $|X^\lambda|$ defines lower variance estimators which have similar properties.

The full vector of empirical scattering moments

$$\phi(X) = (\phi_1(X), \phi_2(X), \phi_3(X), \phi_4(X)), \quad (42)$$

has a dimension $r = O(\log_2^3 d)$. These empirical moments are invariant to translations of X . It results that a maximum entropy distribution conditioned by $m = \mathbb{E}_p[\phi]$ is necessarily stationary. We shall see that the richness of scattering empirical moments is sufficient to insure a quick convergence of the MGD homotopic transport discussed in Section 4.1.

6.3 Generation of Multiscale Time Series in Finance

Financial time series are examples of one-dimensional multiscale sequences with strong non-Gaussian properties, including bursts of activity and time-reversal asymmetry. If $P(u)$ denotes the daily closing price at time u ,

then $X(u) = \log P(u) - \log P(u-1)$ is the corresponding log-return. Figure 6(a) displays S&P 500 daily log-returns from January 2000 to February 2024, a series of $d = 6064$ time steps exhibiting strong intermittency and fat tails. Stochastic models of such time series are crucial for risk management, pricing, and hedging of contingent claims. Often, as with the S&P 500, only a single realization of the process is available.

Wavelet moments can be estimated from empirical sums under the assumption that the increments are stationary and ergodic [19], so that $\phi(X) \approx \mathbb{E}[\phi(X)]$. Figure 6(b) shows a sample X_1^σ generated by MGD with $\sigma^2 = 5.5$, using $r = 217$ empirical wavelet scattering moments (42) computed with the Morlet wavelet of Figure 5(a). The intermittent behavior and bursts are qualitatively reproduced. In the following, we do not analyze the accuracy of this wavelet scattering model, which is studied in [19], but rather focus on the entropy properties of MGD samples as the volatility σ increases.

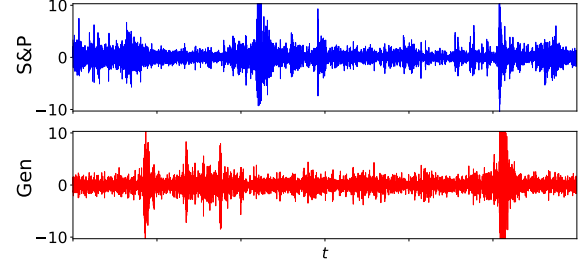


Figure 6: (a) S&P 500 daily log-returns ($d = 6060$) from January 2000 to February 2024. (b) Sample generated by MGD with $\sigma^2 = 5.5$, using $r = 217$ empirical wavelet scattering moments (42) computed from (a). Intermittency is reproduced.

Unlike the numerical examples of Section 5, here the true distribution p of X and the maximum entropy distribution p_* constrained by wavelet scattering moments are unknown. Nor can we compute the entropy $H(p_1^\sigma)$ directly; only the lower bound H_*^σ from (30) is accessible. We therefore test convergence of the sampled density p_1^σ through the entropy lower bound H_*^σ as σ increases.

Figure 7(a) shows that the negentropy estimate $\Delta H_*^\sigma = d^{-1}(H(g) - H_*^\sigma)$ decreases before reaching a plateau for $\sigma^2 \geq 2.5$, indicating that H_*^σ increases and then stabilizes. At $\sigma_{\max}^2 = 5.5$, the negentropy estimate is $\Delta H_*^{\sigma_{\max}} = 0.05$, small compared to other non-Gaussian processes reported in Table 2. This is expected, as Gaussian models are often used as first-order approximations of financial time series. Nevertheless, this negentropy captures non-Gaussian phenomena such as the bursts of activity visible in Figure 6(a).

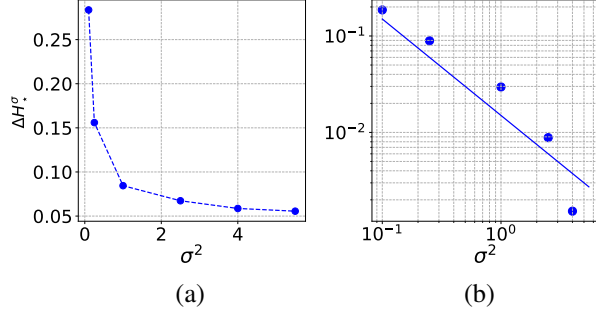


Figure 7: (a) Negentropy estimate ΔH_*^σ from (36) versus σ^2 for S&P 500 log-returns. (b) Convergence of H_*^σ , measured by $d^{-1}(H_*^{\sigma_{\max}} - H_*^\sigma)$ with $\sigma_{\max}^2 = 5.5$, versus σ^2 . The plain line shows σ^{-2} decay.

Figure 7(b) shows the convergence rate of $d^{-1}(H_*^{\sigma_{\max}} - H_*^\sigma)$ as a function of σ^2 , for sufficiently large σ_{\max} . The negentropy estimate ΔH_*^σ converges as $O(\sigma^{-2})$, consistent with Conjecture 4.4. However, since $H(p_*)$ is unknown, we cannot guarantee convergence to $H(p_*)$.

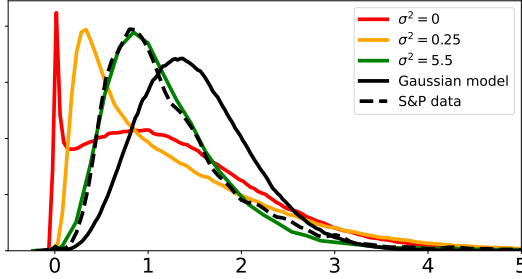


Figure 8: Histograms of rolling volatility $\text{vol}(u)$ computed over $w = 5$ days. Dashed: S&P log-returns X . Red to green: MGD samples X_1^σ for increasing σ^2 . Black: Gaussian process with the same covariance. At $\sigma^2 = 5.5$, the histogram of X_1^σ matches the S&P and differs from the Gaussian.

If the volatility σ is too small, p_1^σ does not reach the maximum entropy density p_* . This manifests as excess intermittency, measured by the rolling volatility of X_1^σ . For zero-mean price increments $X(u)$, the rolling volatility is defined as the local standard deviation over time windows of size w :

$$\text{vol}(u) = \left(w^{-1} \sum_{v=0}^{w-1} |X(u-v)|^2 \right)^{1/2}.$$

Figure 8 shows histograms of rolling volatility: the original S&P increments X (dashed), MGD samples X_1^σ for various σ (coloured), and a Gaussian process (black) having the same quadratic moments $\mathbb{E}[\phi_2(X)]$ as the S&P. The mismatch between the rolling volatility of the S&P and the Gaussian process confirms that the S&P is non-Gaussian.

When σ is too small, the histogram exhibits a sharp peak at low volatility and a heavier tail, indicating stronger

bursts of energy interspersed with more regular variations. At $\sigma^2 = 5.5$, where the entropy H_*^σ has nearly converged to its maximum, the volatility histogram matches that of the S&P increments. This agreement is a partial validation of the model since rolling volatility was not explicitly incorporated into the wavelet scattering model.

6.4 Generation of Two-Dimensional Physical Fields

Similar numerical experiments are performed on two-dimensional physical fields. We consider cosmological and turbulent fluid fields, which are non-Gaussian stationary fields with long-range spatial dependencies and coherent geometric structures. Estimating energy models of out-of-equilibrium systems is central to statistical physics [38, 39].

Original samples are shown in the top row of Figure 9. Figure 9(a) shows a cosmic web field, constructed by extracting a 2D slice from a 3D simulation of the large-scale dark matter distribution [22] with a logarithmic transformation [21]. Figure 9(b) shows a turbulent vorticity field from a 2D incompressible Navier–Stokes simulation [40], with periodic boundary conditions. These fields have dimension $d = 128^2$ and are modelled with $r = 2392$ scattering moments, estimated on batches of 100 replicas in MGD.

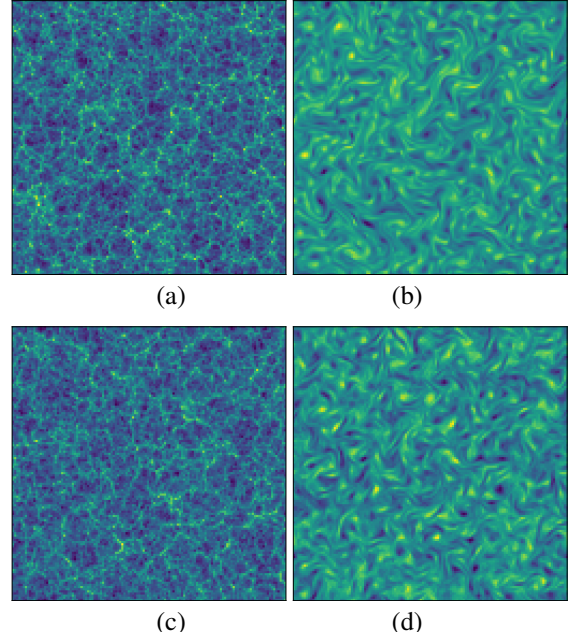


Figure 9: (a) Cosmic web field: 2D slice from a 3D dark matter simulation. (b) Turbulent vorticity field from 2D incompressible Navier–Stokes. Both images are 128×128 pixels. (c,d) MGD samples with wavelet scattering moments at $\sigma^2 = 5.5$.

The samples in Figures 9(c,d), generated by MGD with $\sigma_{\max}^2 = 5.5$, are visually similar to the originals. The quality is comparable to results from the ad-hoc micro-

canonical algorithm of [21], which performs moment matching without controlling entropy.

As for financial time series, we test convergence of p_1^σ through the lower bound H_*^σ of its entropy, via the negentropy estimate $\Delta H_*^\sigma = d^{-1}(H(g) - H_*^\sigma)$. Figure 10(a) shows that ΔH_*^σ decreases and reaches a plateau for $\sigma^2 \geq 2.5$, similar to the S&P time series. Figure 10(b) displays the convergence of H_*^σ by computing $d^{-1}(H_*^{\sigma_{\max}} - H_*^\sigma)$ for $\sigma_{\max}^2 = 5.5$, for turbulence (red) and cosmic web (blue). The decay is proportional to σ^{-2} , supporting Conjecture 4.4.

At $\sigma_{\max}^2 = 5.5$, the negentropy estimate is $\Delta H_*^{\sigma_{\max}} = 0.34$ for turbulence, much larger than $\Delta H_*^{\sigma_{\max}} = 0.07$ for the cosmic web. This reflects the stronger geometric regularity of turbulent fields, with filaments wrapping around vortices—structures that are highly non-Gaussian.

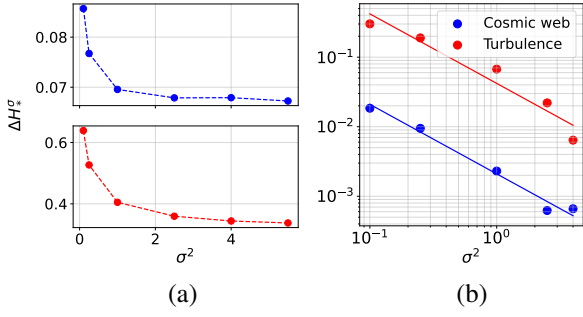


Figure 10: (a) Negentropy estimate ΔH_*^σ from (36) versus σ^2 for cosmic web (blue) and turbulence (red). (b) Convergence of H_*^σ , measured by $d^{-1}(H_*^{\sigma_{\max}} - H_*^\sigma)$ with $\sigma_{\max}^2 = 5.5$, versus σ^2 . Plain lines show σ^{-2} decay.

Table 2: Negentropy estimate ΔH_*^σ at $\sigma = \sigma_{\max}$.

Dataset	Estimated Normalized Negentropy
Laplacian	0.07
S&P 500	0.05
Cosmic Web	0.07
2D Turbulence	0.34

The effect of an excessively small σ is visible in the histograms of fine-scale wavelet coefficients $\text{Re}(X_1^\lambda)$ for $j = 0, \ell = 0$, and $X_1 \sim p_1^\sigma$, which exhibit a spike at zero (Figure 11). As σ increases, this artifact disappears and the histogram converges toward that of the original data, even though this marginal distribution is not imposed by the moment map ϕ .

As with rolling volatility in the one-dimensional setting, increasing σ raises the entropy of the sampled process, which translates into increased entropy of wavelet coefficient marginals. This progressively improves the match with the original data, whose entropy lies below that of the maximum entropy distribution.

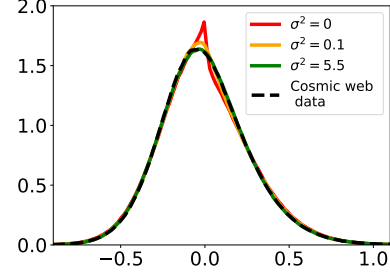


Figure 11: Histograms of finest-scale wavelet coefficients $\text{Re}(X_1^\lambda)$ for $\lambda = \xi$ ($j = 0, \ell = 0$) of cosmic web samples from the scattering MGD model, with $\sigma^2 \in \{0, 0.1, 5.5\}$. Dashed black: original data. All histograms are computed over 500 samples. Larger σ^2 yields better tail reproduction; small σ^2 produce more regular samples which have too many small wavelet coefficients, as in Figure 2(a).

6.5 Convergence with Model Error

The previous experiments consider processes where the maximum entropy model closely approximates the unknown data distribution: $p_* \approx p$. We now consider an example where the model error $D_{\text{KL}}(p \| p_*)$ is large, to verify that MGD can still efficiently sample p_* even when it is a poor approximation of p .

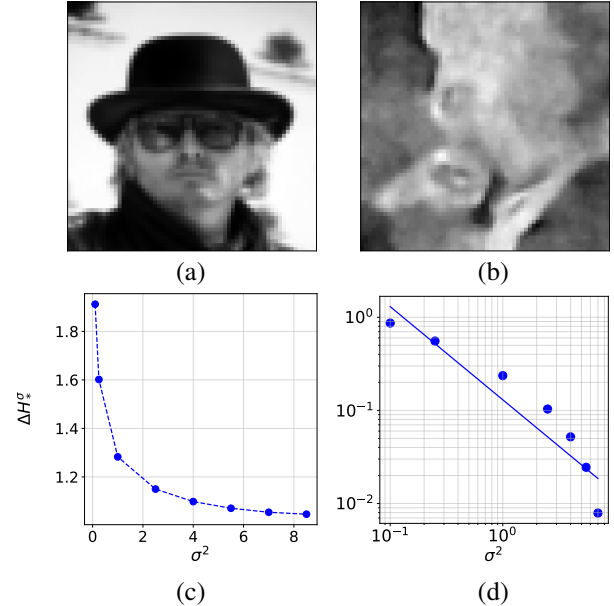


Figure 12: MGD with large model error on CelebA faces (64×64). (a) Original sample. (b) MGD sample with wavelet scattering moments at $\sigma^2 = 1$. (c) Negentropy estimate ΔH_*^σ from (36) versus σ^2 . (d) Convergence of H_*^σ , measured by $d^{-1}(H_*^{\sigma_{\max}} - H_*^\sigma)$ with $\sigma_{\max}^2 = 8.5$; the line shows σ^{-2} decay.

We choose p as a distribution whose samples are centred human faces from the CelebA dataset [41] (Figure 12(a)),

with a ϕ which computes wavelet scattering moments as before. The resulting maximum entropy model p_* is therefore stationary whereas the data distribution is highly non-stationary. Figure 12(b) shows a sample generated by the MGD. It is a sample of a stationary process, which therefore mixes structures across the whole image space. It reproduces edges and regular regions but destroys the face structure. As expected it has a large model error. Nonetheless, MGD converges quickly to p_* .

Figure 12(c) shows that the negentropy estimate ΔH_*^σ reaches a plateau for $\sigma^2 \approx 6$, and Figure 12(d) confirms convergence at rate $O(\sigma^{-2})$. The volatility required for convergence is comparable to the physics and finance examples, confirming that for scattering spectra, MGD reaches the maximum entropy distribution for the same range of σ , regardless of the model error.

7 Conclusion

We introduced Moment-Guided Diffusion (MGD), a sampler for maximum entropy distributions estimated from data. Its homotopic path avoids the computational bottleneck of energy barrier crossing that plagues MCMC methods for non-convex distributions. This represents a paradigm shift in maximum entropy modelling: rather than estimating parameters, MGD directly generates samples from the target distribution. A key by-product is a tractable entropy estimator, which we use to compute the negentropy of complex high-dimensional datasets.

We validated MGD on synthetic examples and real-world data, including financial time series, turbulent vorticity fields, and cosmological dark matter distributions. In all cases, the sampled distributions converge to the target maximum entropy distribution as the volatility σ increases, with entropy gaps decaying as $O(\sigma^{-2})$ across all tested domains. The negentropy estimates reveal the degree of non-Gaussianity and structure in these datasets, providing a principled measure of statistical complexity.

MGD opens promising avenues in computational physics and biology, where it can replace microcanonical samplers [21, 42] or be adapted to molecular dynamics with restraints [43]. More broadly, while our formulation uses an explicit moment map ϕ , the framework naturally accommodates neural network parametrizations, suggesting a principled maximum entropy foundation for diffusion-based generative models.

Several theoretical questions remain open. Although we provide convergence guarantees under specific conditions, a proof of convergence in full generality remains an important challenge. A further question concerns the behaviour of MGD when the maximum entropy distribution constrained by moments $m = \mathbb{E}[\phi(X)]$ does not exist. Another important issue is to understand how the convergence of MGD to the maximum entropy distribution depends upon the choice of the moment generating function ϕ , which needs to be sufficiently flexible. Computing a

moment interpolation path m_t directly from $m = \mathbb{E}_p[\phi]$ and ϕ is also a promising research direction, to apply the MGD to sample maximum entropy distributions, even if we do not have access to samples of p .

Acknowledgments

This work was supported by PR[AI]RIE-PSAI-ANR-23-IACL-0008 and the DRUIDS projet ANR-24-EXMA-0002. It was granted access to the HPC resources of IDRIS under the allocations 2025-AD011016159R1 and 2025-A0181016159 made by GENCI. The authors thank Antonin Chodron de Courcel and Louis-Pierre Chaintron for their fruitful discussions on McKean-Vlasov equations.

References

- [1] E. T. Jaynes, “Information theory and statistical mechanics,” *Physical review*, vol. 106, no. 4, p. 620, 1957.
- [2] I. Goodfellow, J. Pouget-Abadie, M. Mirza, B. Xu, D. Warde-Farley, S. Ozair, A. Courville, and Y. Bengio, “Generative adversarial networks,” *Communications of the ACM*, vol. 63, no. 11, pp. 139–144, 2020.
- [3] Y. Lipman, R. T. Q. Chen, H. Ben-Hamu, M. Nickel, and M. Le, “Flow matching for generative modeling,” 2023. [Online]. Available: <https://arxiv.org/abs/2210.02747>
- [4] M. S. Albergo and E. Vanden-Eijnden, “Building normalizing flows with stochastic interpolants,” 2022. [Online]. Available: <https://arxiv.org/abs/2209.15571>
- [5] M. S. Albergo, N. M. Boffi, and E. Vanden-Eijnden, “Stochastic interpolants: A unifying framework for flows and diffusions,” *arXiv preprint arXiv:2303.08797*, 2023.
- [6] J. Ho, A. Jain, and P. Abbeel, “Denoising diffusion probabilistic models,” *Advances in neural information processing systems*, vol. 33, pp. 6840–6851, 2020.
- [7] Y. Song, J. Sohl-Dickstein, D. P. Kingma, A. Kumar, S. Ermon, and B. Poole, “Score-based generative modeling through stochastic differential equations,” in *International Conference on Learning Representations*, 2021. [Online]. Available: <https://openreview.net/forum?id=PxTIG12RRHS>
- [8] C.-H. Lai, Y. Song, D. Kim, Y. Mitsufuji, and S. Ermon, “The principles of diffusion models,” *arXiv preprint arXiv:2510.21890*, 2025.
- [9] S. Kullback, *Information theory and statistics*. Courier Corporation, 1997.
- [10] T. M. Cover, *Elements of information theory*. John Wiley & Sons, 1999.

[11] C. M. Bishop, *Pattern recognition and machine learning by Christopher M. Bishop*. Springer Science+ Business Media, LLC Berlin, Germany, 2006, vol. 400.

[12] J. Zinn-Justin, *Quantum field theory and critical phenomena*. Oxford university press, 2021, vol. 171.

[13] A. D. Sokal, “How to beat critical slowing-down: 1990 update,” *Nuclear Physics B-Proceedings Supplements*, vol. 20, pp. 55–67, 1991.

[14] X. Liu, C. Gong, and Q. Liu, “Flow straight and fast: Learning to generate and transfer data with rectified flow,” 2022. [Online]. Available: <https://arxiv.org/abs/2209.03003>

[15] Z. Kadkhodaie, F. Guth, E. P. Simoncelli, and S. Mallat, “Generalization in diffusion models arises from geometry-adaptive harmonic representations,” in *The Twelfth International Conference on Learning Representations*, 2024. [Online]. Available: <https://openreview.net/forum?id=ANvmVS2Yr0>

[16] E. Schrödinger, *What is Life? The Physical Aspect of the Living Cell*. Cambridge University Press, 1944.

[17] A. Hyvärinen and P. Dayan, “Estimation of non-normalized statistical models by score matching,” *Journal of Machine Learning Research*, vol. 6, no. 4, 2005.

[18] J. Bruna and S. Mallat, “Multiscale sparse microcanonical models,” *Mathematical Statistics and Learning*, vol. 1, no. 3, pp. 257–315, 2019.

[19] R. Morel, G. Rochette, R. F. Leonarduzzi, J.-P. Bouchaud, and S. Mallat, “Scale dependencies and self-similarity through wavelet scattering covariance,” *ArXiv*, vol. abs/2204.10177, 2022. [Online]. Available: <https://api.semanticscholar.org/CorpusID:248299807>

[20] A. Brochard and S. Zhang, “Generalized rectifier wavelet covariance models for texture synthesis,” in *International Conference on Learning Representations*, 2022. [Online]. Available: https://openreview.net/forum?id=ziRLU3Y2PN_

[21] S. Cheng, R. Morel, E. Ally, B. M’enard, and S. Mallat, “Scattering spectra models for physics,” *PNAS Nexus*, vol. 3, 2023. [Online]. Available: <https://api.semanticscholar.org/CorpusID:259309140>

[22] F. Villaescusa-Navarro, C. Hahn, E. Massara, A. Banerjee, A. M. Delgado, D. K. Ramanah, T. Charnock, E. Giusarma, Y. Li, E. Ally *et al.*, “The quijote simulations,” *The Astrophysical Journal Supplement Series*, vol. 250, no. 1, p. 2, 2020.

[23] K. Schneider, J. Ziuber, M. Farge, and A. Azzalini, “Coherent vortex extraction and simulation of 2d isotropic turbulence,” *Journal of Turbulence*, no. 7, p. N44, 2006.

[24] C. P. Robert, G. Casella, and G. Casella, *Monte Carlo statistical methods*. Springer, 1999, vol. 2.

[25] P. E. Kloeden and R. Pearson, “The numerical solution of stochastic differential equations,” *The ANZIAM Journal*, vol. 20, no. 1, pp. 8–12, 1977.

[26] D. J. Higham, “An algorithmic introduction to numerical simulation of stochastic differential equations,” *SIAM review*, vol. 43, no. 3, pp. 525–546, 2001.

[27] J. Besag, “Comments on “representations of knowledge in complex systems” by u. grenander and mi miller,” *J. Roy. Statist. Soc. Ser. B*, vol. 56, no. 591–592, p. 4, 1994.

[28] S. Chewi, M. A. Erdogdu, M. Li, R. Shen, and M. S. Zhang, “Analysis of langevin monte carlo from poincare to log-sobolev,” *Foundations of Computational Mathematics*, vol. 25, no. 4, pp. 1345–1395, 2025.

[29] R. Li, H. Zha, and M. Tao, “Sqrt(d) dimension dependence of langevin monte carlo,” in *International Conference on Learning Representations*, 2022. [Online]. Available: https://openreview.net/forum?id=5-2mX9_U5i

[30] F. Koehler, A. Heckett, and A. Risteski, “Statistical efficiency of score matching: The view from isoperimetry,” *arXiv preprint arXiv:2210.00726*, 2022.

[31] T. Bonnaire, R. Urfin, G. Biroli, and M. Mezard, “Why diffusion models don’t memorize: The role of implicit dynamical regularization in training,” in *The Thirty-ninth Annual Conference on Neural Information Processing Systems*, 2025. [Online]. Available: <https://openreview.net/forum?id=BSZqpqgqM0>

[32] A. Favero, A. Sclocchi, and M. Wyart, “Bigger isn’t always memorizing: Early stopping overparameterized diffusion models,” 2025. [Online]. Available: <https://arxiv.org/abs/2505.16959>

[33] H. P. McKean Jr, “A class of markov processes associated with nonlinear parabolic equations,” *Proceedings of the National Academy of Sciences*, vol. 56, no. 6, pp. 1907–1911, 1966.

[34] L.-P. Chaintron and A. Diez, “Propagation of chaos: a review of models, methods and applications. i. models and methods,” *arXiv preprint arXiv:2203.00446*, 2022.

[35] G. O. Roberts and J. S. Rosenthal, “Optimal scaling of discrete approximations to langevin diffusions,” *Journal of the Royal Statistical Society: Series B (Statistical Methodology)*, vol. 60, no. 1, pp. 255–268, 1998.

[36] S. Mallat, “Group invariant scattering,” *Communications on Pure and Applied Mathematics*, vol. 65, no. 10, pp. 1331–1398, 2012.

[37] ———, *A wavelet tour of signal processing*. Elsevier, 1999.

- [38] A. Brossollet, E. Lempereur, S. Mallat, and G. Biroli, “Effective energy, interactions and out of equilibrium nature of scalar active matter,” *Communications Physics*, 2025.
- [39] N. M. Boffi and E. Vanden-Eijnden, “Deep learning probability flows and entropy production rates in active matter,” *Proceedings of the National Academy of Sciences*, vol. 121, no. 25, p. e2318106121, 2024.
- [40] K. Schneider, J. Ziuber, M. Farge, and A. Azzalini, “Coherent vortex extraction and simulation of 2d isotropic turbulence,” *Journal of Turbulence*, vol. 7, p. N44, 2006. [Online]. Available: <https://doi.org/10.1080/14685240600601061>
- [41] Z. Liu, P. Luo, X. Wang, and X. Tang, “Deep learning face attributes in the wild,” in *Proceedings of International Conference on Computer Vision (ICCV)*, December 2015.
- [42] E. Ally, F. Boulanger, F. Levrier, S. Zhang, C. Colling, B. Regaldo-Saint Blanchard, P. Hennebelle, and S. Mallat, “The RWST, a comprehensive statistical description of the non-Gaussian structures in the ISM,” *Astronomy & Astrophysics - A&A*, vol. 629, p. A115, 2019. [Online]. Available: <https://cea.hal.science/cea-02290738>
- [43] B. Roux and J. Weare, “On the statistical equivalence of restrained-ensemble simulations with the maximum entropy method,” *The Journal of chemical physics*, vol. 138, no. 8, 2013.
- [44] P. D. Welch, “The use of fast fourier transform for the estimation of power spectra: A method based on time averaging over short, modified periodograms,” *IEEE Transactions on Audio and Electroacoustics*, vol. 15, pp. 70–73, 1967. [Online]. Available: <https://api.semanticscholar.org/CorpusID:13900622>

A Proofs

In this appendix, we prove Theorem 3.1, Proposition 4.3, and the additional Proposition A.1, which shows that the entropy increases along MGD’s dynamic when the moments are fixed ($dm_t/dt = 0$). For the reader’s convenience we state again the results from main text.

Theorem 3.1 (Moment Guided Diffusion). *Consider the SDE*

$$dX_t = (\eta_t^\top - \sigma^2 \theta_t^\top) \nabla \phi(X_t) dt + \sqrt{2} \sigma dW_t, \quad X_0 = Z, \quad (13)$$

where W_t is a Brownian noise and η_t and θ_t solve

$$G_t \eta_t = \frac{d}{dt} m_t, \quad (14)$$

$$G_t \theta_t = \mathbb{E}[\Delta \phi(X_t)], \quad (15)$$

where G_t is the Gram matrix

$$G_t = \mathbb{E}[\nabla \phi(X_t) \cdot \nabla \phi(X_t)^\top]. \quad (16)$$

If this coupled system admits a solution, then the moment condition $\mathbb{E}[\phi(X_t)] = m_t$ holds for all $t \in [0, 1]$.

Proof. By Ito’s lemma

$$\begin{aligned} d\phi(X_t) &= \nabla \phi(X_t) dX_t + \sigma^2 \Delta \phi(X_t) dt \\ &= \nabla \phi(X_t) \cdot \nabla \phi(X_t)^\top (\eta_t - \sigma^2 \theta_t) dt \\ &\quad + \sigma^2 \Delta \phi(X_t) dt + \sqrt{2} \sigma \nabla \phi(X_t) \cdot dW_t. \end{aligned}$$

Taking the expected value of this equation we obtain that

$$\begin{aligned} \frac{d}{dt} \mathbb{E}[\phi(X_t)] &= \mathbb{E}[\nabla \phi(X_t) \cdot \nabla \phi(X_t)^\top] (\eta_t - \sigma^2 \theta_t) \\ &\quad + \sigma^2 \mathbb{E}[\Delta \phi(X_t)]. \end{aligned}$$

Since we require that $\mathbb{E}[\phi(X_t)] = \mathbb{E}[\phi(I_t)] = m_t$ for all $t \in [0, 1]$, we must also have

$$\frac{d}{dt} \mathbb{E}[\phi(X_t)] = \frac{d}{dt} m_t$$

Combining these two last equations we deduce that

$$G_t (\eta_t - \sigma^2 \theta_t) + \sigma^2 \mathbb{E}[\Delta \phi(X_t)] = \frac{d}{dt} m_t,$$

where $G_t = \mathbb{E}[\nabla \phi(X_t) \cdot \nabla \phi(X_t)^\top]$. This equation is satisfied since η_t and θ_t are solutions to (14) and (15), respectively. Therefore $\frac{d}{dt} \mathbb{E}[\phi(X_t)] = \frac{d}{dt} m_t$ which implies that

$$\forall t \in [0, 1] : \mathbb{E}[\phi(X_t)] = m_t$$

since $\mathbb{E}[\phi(X_0)] = m_0$. \square

Proposition 4.3. *Assume the MGD SDE (13) admits a unique strong solution for all $t \in [0, 1]$. Then,*

$$\begin{aligned} \frac{d}{dt} H(p_t^\sigma) &= \theta_t^\top \frac{d}{dt} m_t \\ &\quad + \sigma^2 \mathbb{E}[|\nabla \log p_t^\sigma(X_t) + \theta_t^\top \nabla \phi(X_t)|^2], \end{aligned} \quad (28)$$

and hence

$$\frac{d}{dt} H(p_t^\sigma) \geq \theta_t^\top \frac{d}{dt} m_t. \quad (29)$$

Proof: The PDF p_t^σ of the solution to the MGD SDE (13) for a given $\sigma \geq 0$ obeys the Fokker-Planck Equation

$$\partial_t p_t^\sigma = \nabla ((-\eta_t + \sigma^2 \theta_t)^\top \nabla \phi p_t^\sigma) + \sigma^2 \Delta p_t^\sigma.$$

We use this equation to derive an evolution equation for the relative entropy $H(p_t^\sigma)$. and some integrations by part

$$\begin{aligned} \frac{d}{dt} H(p_t^\sigma) &= - \int \partial_t p_t^\sigma \log p_t^\sigma dx - \int \partial_t p_t^\sigma dx \\ &= - \int \nabla \cdot ((-\eta_t + \sigma^2 \theta_t)^\top \nabla \phi p_t^\sigma) \log p_t^\sigma dx \\ &\quad - \sigma^2 \int \Delta p_t \log p_t^\sigma dx \\ &= \int ((-\eta_t + \sigma^2 \theta_t)^\top \nabla \phi \cdot \nabla p_t^\sigma) dx \\ &\quad + \sigma^2 \int \nabla \log p_t^\sigma \cdot \nabla p_t^\sigma dx \\ &= \int ((\eta_t - \sigma^2 \theta_t)^\top \Delta \phi + \sigma^2 |\nabla \log p_t^\sigma|^2) p_t^\sigma dx, \end{aligned}$$

where we used a few integration by parts and the identity $p_t^\sigma \nabla \log p_t^\sigma = \nabla p_t^\sigma$. Writing the integral in the last equation as an expectation, we deduce that

$$\frac{d}{dt} H(p_t^\sigma) = (\eta_t - \sigma^2 \theta_t)^\top \mathbb{E}[\Delta \phi(X_t)] + \sigma^2 \mathbb{E}[|\nabla \log p_t^\sigma(X_t)|^2].$$

Using $G_t \theta_t = \mathbb{E}[\Delta \phi(X_t)]$ from (15), we obtain that

$$\begin{aligned} \mathbb{E}[|\nabla \log p_t^\sigma(X_t)|^2] &= \mathbb{E}[|\nabla \log p_t^\sigma(X_t) + \theta_t^\top \nabla \phi(X_t)|^2] \\ &\quad - 2\mathbb{E}[|\nabla \log p_t^\sigma(X_t) \cdot \theta_t^\top \nabla \phi(X_t)|] \\ &\quad - \mathbb{E}[|\theta_t^\top \nabla \phi(X_t)|^2] \\ &= \mathbb{E}[|\nabla \log p_t^\sigma(X_t) + \theta_t^\top \nabla \phi(X_t)|^2] \\ &\quad + 2\theta_t^\top \mathbb{E}[\Delta \phi(X_t)] \\ &\quad - \theta_t^\top \mathbb{E}[\nabla \phi(X_t) \cdot \nabla \phi(X_t)^\top] \\ &= \mathbb{E}[|\nabla \log p_t^\sigma(X_t) + \theta_t^\top \nabla \phi(X_t)|^2] \\ &\quad + 2\theta_t^\top \mathbb{E}[\Delta \phi(X_t)] - \theta_t^\top G_t \theta_t \\ &= \mathbb{E}[|\nabla \log p_t^\sigma(X_t) + \theta_t^\top \nabla \phi(X_t)|^2] \\ &\quad + \theta_t^\top \mathbb{E}[\Delta \phi(X_t)]. \end{aligned}$$

Combining these last two equation, we deduce that

$$\begin{aligned} \frac{d}{dt} H(p_t^\sigma) &= \eta_t \mathbb{E}[\Delta \phi(X_t)] + \sigma^2 \mathbb{E}[|\nabla \log p_t^\sigma(X_t)|^2] \\ &= \eta_t^\top G_t \theta_t + \sigma^2 \mathbb{E}[|\nabla \log p_t^\sigma(X_t)|^2] \\ &\geq \eta_t^\top G_t \theta_t. \end{aligned}$$

Finally, since $G_t \eta_t = dm_t/dt$ from (14), we arrive at

$$\frac{d}{dt} H(p_t^\sigma) \geq \theta_t^\top \frac{d}{dt} m_t.$$

□

This proposition shows that $\frac{d}{dt} H(p_t^\sigma) \geq 0$ if $dm_t/dt = 0$ (i.e. if the moments are preserved). Our next proposition shows that in that setup the entropy also increases as a function of the volatility σ at any given time t .

Proposition A.1. *Let p_t^σ be the PDF of the solution to the MGD SDE (13). If we assume that $dm_t/dt = 0$, then at any time $t \in (0, 1]$, we have*

$$\frac{d}{d\sigma} H(p_t^\sigma) \geq 0. \quad (43)$$

Proof. Since $dm_t/dt = 0$, Proposition 4.3 implies that, for all $\sigma > 0$,

$$\frac{d}{dt} H(p_t^\sigma) \geq 0.$$

Because $\eta_t = 0$ when $dm_t/dt = 0$ by (14), in this setup the Fokker-Planck equation for p_t^σ reduces to

$$\partial_t p_t^\sigma = \sigma^2 \nabla(\theta_t^\top \nabla \phi p_t^\sigma) + \sigma^2 \Delta p_t^\sigma.$$

By rescaling time as $\tau = t\sigma^2$, we see from this equation that

$$p_t^\sigma = p_\tau^{\sigma=1}.$$

Therefore

$$\frac{d}{d\sigma} H(p_t^\sigma) = \frac{2\tau}{\sigma} \frac{d}{d\tau} H(p_\tau^{\sigma=1}),$$

$$\frac{d}{d\sigma} H(p_t^\sigma) \geq 0.$$

□

B Conjectures

In this appendix, we support Conjectures 4.1 and 4.4 by performing a Taylor expansion of the Fokker-Planck equation (22). This formal derivation provides convergence rates for the entropy of the MGD solution and its lower bound towards the entropy of the maximum entropy distribution. Let us write the Fokker-Planck Equation for the MGD SDE (13) as

$$\sigma^{-2} \partial_t p_t^\sigma = \nabla \cdot (p_t^\sigma ((-\sigma^{-2} \eta_t + \theta_t)^\top \nabla \phi)) + \Delta p_t^\sigma.$$

When σ goes to infinity, we expect $\sigma^{-2} \partial_t p_t^\sigma$ and $\sigma^{-2} \eta_t$ to vanish. Assuming that η_t , θ_t , and p_t^σ admit a limit as σ goes to infinity, and denoting

$$\lim_{\sigma \rightarrow \infty} p_t^\sigma = p_t^* \text{ and } \lim_{\sigma \rightarrow \infty} \theta_t = \theta_t^*,$$

the Fokker-Planck Equation gives

$$0 = \nabla \cdot (p_t^* (\theta_t^* \nabla \phi)) + \Delta p_t^*.$$

The solution to this equation is

$$p_t^*(x) = e^{-\theta_t^{*\top} \phi(x)} / \mathcal{Z}_t^*,$$

for $\mathcal{Z}_t^* = \int e^{-\theta_t^{*\top} \phi(x)} dx$. Taking the limit as $\sigma \rightarrow \infty$ in the moments equality, we obtain

$$\int \phi(x) p_t^*(x) dx = \lim_{\sigma \rightarrow \infty} \int \phi(x) p_t^\sigma(x) dx = m_t.$$

This shows that the distribution with density p_t^* is exponential, with moments m_t . Therefore, p_t^* is the unique maximizer of the entropy $H(q)$, under the constraints $\mathbb{E}_q[\phi] = \mathbb{E}[\phi(I_t)]$, and θ_t^* are the associated Lagrange multipliers. This also implies that $p_{t-1}^* = p_*$ and $\theta_{t-1}^* = \theta_*$.

The term led by σ^{-2} in the Fokker-Planck Equation suggests to Taylor expand p_t^σ in σ^{-2} :

$$p_t^\sigma(x) = p_t^*(x) (1 + \sigma^{-2} q_t(x) + o(\sigma^{-2})).$$

Injecting this expansion in the entropy of p_t^σ , we obtain

$$\begin{aligned} H(p_t^\sigma) - H(p_t^*) &= -\sigma^{-2} \int q_t(x) p_t^*(x) dx + o(\sigma^{-2}) \\ &= o(\sigma^{-2}) \end{aligned}$$

where we used $\int q_t p_t^* dx = 0$, which follows from integrating the expansion for p_t^σ above since $\int p_t^\sigma dx = \int p_t^* dx = 1$. As a consequence,

$$|H(p_t^\sigma) - H(p_t^*)| = o(\sigma^{-2}) \leq C \sigma^{-2}$$

for some C . At $t = 1$, since $p_{t=1}^* = p_*$, we recover (25) for Conjecture 4.1.

Assuming that we can also perform an asymptotic expansion for θ_t :

$$\theta_t = \theta_t^* + \sigma^{-2}\tilde{\theta}_t + o(\sigma^{-2}),$$

we deduce that the lower bound (30) follows

$$\begin{aligned} \int_0^1 \theta_t^\top \frac{d}{dt} m_t dt &= \int_0^1 \theta_t^* \top \frac{d}{dt} m_t dt \\ &\quad + \sigma^{-2} \int_0^1 \tilde{\theta}_t^\top \frac{d}{dt} m_t dt + o(\sigma^{-2}). \end{aligned}$$

We also deduce that the Fisher divergence vanishes as $o(\sigma^{-2})$ since

$$\begin{aligned} \sigma^2 \mathbb{E} [|\nabla \log p_t^\sigma(X_t) + \theta_t^\top \nabla \phi|^2] &= \sigma^2 \mathbb{E} [|\nabla \log(p_t^\sigma/p_1^*)(X_t) + (\theta_t - \theta_t^*)^\top \nabla \phi(X_t)|^2] \\ &= \sigma^2 \mathbb{E} [|\sigma^{-2} \nabla q_t(X_t) + \sigma^{-2} \tilde{\theta}_t^\top \nabla \phi(X_t) + o(\sigma^{-2})|^2] \\ &= \sigma^{-2} \mathbb{E} [|\nabla q_t(X_t) + \tilde{\theta}_t^\top \nabla \phi(X_t) + o(1)|^2] \\ &= O(\sigma^{-2}). \end{aligned}$$

Therefore, if we denote

$$H_*^\sigma = H(p_0) + \int_0^1 \theta_t^\top \frac{d}{dt} m_t dt,$$

from (28) we formally deduce that there exists C' such that

$$|H_*^\sigma - H(p_*)| = \sigma^{-2} C'.$$

The entropy lower bound $H_*^\sigma \leq H(p_1^\sigma)$ thus converges towards $H(p_*)$ as $O(\sigma^{-2})$ as suggested in (32) of Conjecture 4.4.

C Alternative Numerical Implementations

Algorithm 1 computes η_t and θ_t on-the-fly using the current particle ensemble. This section describes two alternatives that may be preferable depending on the application: the first prioritizes speed and scalability, while the second preserves the interpretation of η_t and θ_t as intrinsic parameters of the generative model.

C.1 Precomputed Transport via Interpolant Regression

The MGD SDE (13) can also be written as

$$dX_t = \lambda_t^\top \nabla \phi(X_t) dt + \sqrt{2}\sigma dW_t \quad (44)$$

where λ_t is a Lagrange multiplier used to enforce $\mathbb{E}[\phi(X_t)] = m_t$. That is, the decomposition $\lambda_t = \eta_t - \sigma^2 \theta_t$ used in text is not unique. In particular, we can also use $\lambda_t = \tilde{\eta}_t - \sigma^2 \tilde{\theta}_t$, with $\tilde{\eta}_t$ computed using the Gram matrix evaluated on the interpolant I_t rather than on the particles X_t . This changes the predictor step in Algorithm 1, but the corrector step still enforces exact moment

preservation. It allows precomputation of $\tilde{\eta}_t$ before sampling.

Specifically, instead of solving $G_t \eta_t = \frac{d}{dt} m_t$ while sampling, we can precompute $\tilde{\eta}_t$ via solution of the regression problem:

$$\tilde{\eta}_t = \arg \min_{\hat{\eta}_t} \mathbb{E} [|\hat{\eta}_t^\top \nabla \phi(I_t) - \dot{I}_t|^2], \quad (45)$$

where $\dot{I}_t = \frac{d}{dt} I_t$. This can be solved by SGD without matrix inversion, using mini-batches of fresh samples $Z \sim \mathcal{N}(0, \text{Id})$:

$$\tilde{\eta}_t^{k+1} = \tilde{\eta}_t^k - h \mathbb{E} [\nabla \phi(I_t) \cdot ((\tilde{\eta}_t^k)^\top \nabla \phi(I_t) - \dot{I}_t)]. \quad (46)$$

Variants such as Adam or L-BFGS can also be used. The resulting scheme is summarized in Algorithm 2. Note that this algorithm still requires to solve a linear system to obtain $\tilde{\theta}_k$, but this too could be modified by solving

$$\frac{1}{n_{\text{rep}}} \sum_{i=1}^{n_{\text{rep}}} \phi(y_k^i - h \sigma^2 \tilde{\theta}_k^\top \nabla \phi(y_k^i)) - m_{(k+1)h} = 0$$

for $\tilde{\theta}_k$ differently.

Algorithm 2 MGD with Precomputed Transport

Input: volatility σ ; number of steps n_σ ; time step $h = 1/n_\sigma$; number of replicas n_{rep} ; moments $m_t = \mathbb{E}[\phi(I_t)]$

Precomputation: On the time grid $\{t_j = \frac{j}{n_\sigma}\}_{j=0}^{n_\sigma}$, solve (45) via SGD to obtain $\{\eta_{t_j}\}$

Initialize: $x_0^i \sim \mathcal{N}(0, \text{Id})$ for $i = 1, \dots, n_{\text{rep}}$

for $k = 0, \dots, n_\sigma - 1$ **do**

Predictor (using precomputed η_{t_k})

for $i = 1, \dots, n_{\text{rep}}$ **do**

Sample $\xi_k^i \sim \mathcal{N}(0, \text{Id})$

Set $y_k^i = x_k^i + h \tilde{\eta}_{t_k}^\top \nabla \phi(x_k^i) + \sqrt{2h\sigma} \xi_k^i$

end for

Corrector (project to preserve moments)

Compute $\hat{G}'_k = \frac{1}{n_{\text{rep}}} \sum_{i=1}^{n_{\text{rep}}} \nabla \phi(y_k^i) \cdot \nabla \phi(y_k^i)^\top$

Solve $h\sigma^2 \hat{G}'_k \tilde{\theta}_k = \frac{1}{n_{\text{rep}}} \sum_{i=1}^{n_{\text{rep}}} \phi(y_k^i) - m_{(k+1)h}$ for $\tilde{\theta}_k$

for $i = 1, \dots, n_{\text{rep}}$ **do**

Set $x_{k+1}^i = y_k^i - h \sigma^2 \tilde{\theta}_k^\top \nabla \phi(y_k^i)$

end for

end for

Output: Samples $(x_{n_\sigma}^i)_{1 \leq i \leq n_{\text{rep}}}$

C.2 Offline Learning of Coefficients

If the coefficients η_t and θ_t are of intrinsic interest, one can learn them in a preprocessing phase on a time grid, then sample by propagating one particle at a time using these fixed coefficients. This trades computation time for memory and enables fully parallel sampling.

The coefficients are built sequentially: use η_t, θ_t to propagate particles to time $t + \Delta t$, collect statistics to estimate the Gram matrix at this new time, then compute $\eta_{t+\Delta t}, \theta_{t+\Delta t}$,

$\theta_{t+\Delta t}$. Crucially, the Gram matrix can be estimated by accumulating contributions one particle (or batch) at a time, without storing all positions simultaneously. The procedure is summarized in Algorithm 3.

Algorithm 3 MGD with Offline Coefficient Learning

Input: volatility σ ; number of steps n_σ ; time step $h = 1/n_\sigma$; number of replicas n_{rep} ; moments $m_t = \mathbb{E}[\phi(I_t)]$

Learning phase:

Compute $\hat{G}_0 = \frac{1}{n_{\text{rep}}} \sum_{i=1}^{n_{\text{rep}}} \nabla \phi(z^i) \cdot \nabla \phi(z^i)^\top$ with $z^i \sim \rho_0$

Solve for $\hat{\eta}_0, \hat{\theta}_0$

for $k = 1, \dots, n_\sigma$ **do**

 Initialize accumulator $\hat{G}_k = 0$

for batch $b = 1, \dots, B$ **do**

 Propagate n_b particles from $t = 0$ to $t = kh$ using $\{\hat{\eta}_\ell, \hat{\theta}_\ell\}_{\ell < k}$

 Accumulate: $\hat{G}_k \leftarrow \hat{G}_k + \frac{1}{n_b} \sum_{i=1}^{n_b} \nabla \phi(x_k^i) \cdot \nabla \phi(x_k^i)^\top$

end for

 Normalize $\hat{G}_k \leftarrow \frac{1}{B} \hat{G}_k$ and solve for $\hat{\eta}_k, \hat{\theta}_k$

end for

Sampling phase: (can be done one particle at a time)

Initialize $x_0 \sim \mathcal{N}(0, \text{Id})$

for $k = 0, \dots, n_\sigma - 1$ **do**

 Sample $\xi_k \sim \mathcal{N}(0, \text{Id})$

 Set $x_{k+1} = x_k + h(\hat{\eta}_k - \sigma^2 \hat{\theta}_k)^\top \nabla \phi(x_k) + \sqrt{2h\sigma} \xi_k$

end for

Output: Samples $(x_{n_\sigma}^i)_{1 \leq i \leq n_{\text{rep}}}$

D Experimental details

This appendix reviews experimental details of the numerical experiments performed in Sections 5 and 6. In all experiments, the number of steps required by MGD to reach convergence increases with σ , ranging from 10^3 to 10^4 .

D.1 Regularisation

Algorithm 1 requires inverting empirical Gram matrices, which we stabilize through a simple regularization procedure. First, we discard any potential ϕ_k satisfying

$$\frac{1}{m} \sum_{i=1}^m \nabla \phi_k(x^i) \cdot \nabla \phi_k(x^i)^\top = 0, \quad (47)$$

as these correspond to vanishing Lagrange multipliers in p_* (for the scattering spectra case, symmetries produce exact zeros [21]). We then normalize the remaining potentials by their empirical norm, setting the Gram matrix diagonal to unity so that all potentials contribute at comparable scale. Finally, we add a small regularization δId with $\delta = 10^{-7}$ before inversion.

D.2 Entropy and D_{KL} Estimation

In Section 5, we estimate entropies and Kullback–Leibler divergences from one-dimensional histograms. We use $n_{\text{rep}} = 10^6$ replicas and $n_\sigma = 10^4$ discretization steps for MGD, except for the right column of Figure 2 where up to $n_\sigma = 3.10^5$ discretization steps were used. Histograms are constructed from $n_{\text{quantiles}} = 500$ quantiles, yielding discrete density estimates from which we compute the entropies and divergences.

D.3 Financial Time Series and Physical Fields

The S&P time series is preprocessed following [19], Appendix E. Cosmic web fields are 2D slices from 3D dark matter simulations [22] with a logarithmic transformation, as described in [21], Appendix G. Turbulent vorticity fields are obtained from 2D incompressible Navier–Stokes simulations [40]. All signals are standardized, and covariance determinants for negentropy estimation are computed via Welch’s method [44].

Figures 7, 10 and 12 show convergence of the negentropy estimator ΔH_*^σ for $\sigma^2 \in \{0.1, 0.25, 1, 2.5, 4, 5.5\}$, using $m = 100$ particles. The number of discretization steps is adapted to each dataset and volatility (in order of increasing σ^2): S&P uses $\{1000, 1000, 1200, 1200, 2200, 2500\}$, cosmic web $\{1000, 1000, 1000, 1000, 2500, 2700\}$, 2D turbulence $\{1000, 1000, 1000, 1000, 2000, 3300\}$, and CelebA $\{1500, 1500, 2500, 4000, 4000, 6000\}$. For CelebA, we also consider $\sigma^2 = 7$ and $\sigma^2 = 8.5$, respectively computed with 6000 and 7000 steps. Convergence is verified by moment matching throughout the dynamics and confirming stability under additional steps.

The histograms in Figures 8 and 11 use 500 samples for $\sigma^2 \in \{0, 0.1, 5.5\}$, with 1000 discretization steps for $\sigma^2 = 0$.

E The Case of a Quadratic Function ϕ

If ϕ is a quadratic function, $\phi(x) = (x_i x_j)_{1 \leq i \leq j \leq d}$, where x_i is the i -th coordinate of $x \in \mathbb{R}^d$, we know that the maximum entropy distribution is a Gaussian distribution with a covariance that matches the one of the data. In this setup, the MGD SDE (13) takes a simple form, and can be solved analytically. We use this example to illustrate the role of the volatility σ . For simplicity we consider the case of centred distributions: the calculations below can be straightforwardly generalized to situations where the base and the target distribution have a non-zero mean, and the function ϕ also include a linear component. Our first result is:

Theorem E.1. *Assume that the base and the target distributions have zero mean and positive-definite covariance matrices C_0 and C_1 , respectively, and let*

$$C_t = \cos^2(\alpha_t) C_0 + \sin^2(\alpha_t) C_1 \quad (48)$$

be the covariance of the stochastic interpolant $I_t = \cos(\alpha_t)Z + \sin(\alpha_t)X$. Then the MGD SDE (13) associ-

ated with the quadratic function $\phi(x) = (x_i x_j)_{1 \leq i \leq j \leq d}$ reads

$$dX_t = \left(\frac{1}{2} \dot{C}_t C_t^{-1} - \sigma^2 C_t^{-1} \right) X_t dt + \sqrt{2} \sigma dW_t, \quad (49)$$

with $X_0 = Z$ and where $\dot{C}_t = dC_t/dt$.

The proof of this theorem is given at the end of this Appendix. Note that it implies that here we have

$$\begin{aligned} \eta_t^\top \nabla \phi(x) &= \frac{1}{2} \dot{C}_t C_t^{-1} x, \\ \theta_t^\top \nabla \phi(x) &= C_t^{-1} \end{aligned}$$

Since then MGD SDE (49) is linear with additive noise, if Z_0 is Gaussian, its solution is also Gaussian, with mean zero and covariance $\mathbb{E}[X_t X_t^\top] = C_t$ for any $\sigma \geq 0$; indeed a direct calculation with Itô formula shows that

$$\begin{aligned} \frac{d}{dt} \mathbb{E}[X_t X_t^\top] &= \left(\frac{1}{2} \dot{C}_t C_t^{-1} - \sigma^2 C_t^{-1} \right) \mathbb{E}[X_t X_t^\top] \\ &\quad + \mathbb{E}[X_t X_t^\top] \left(\frac{1}{2} C_t^{-1} \dot{C}_t - \sigma^2 C_t^{-1} \right) \\ &\quad + 2\sigma^2 \text{Id}, \end{aligned}$$

whose unique solution is $\mathbb{E}[X_t X_t^\top] = C_t$. That is, in this case X_t has the same law as I_t , and exactly samples the maximum entropy distribution associated with the quadratic ϕ at time $t = 1$. Interestingly, this result also holds if the base distribution is non-Gaussian, provided that we let $\sigma \rightarrow \infty$.

Theorem E.2. *Given any base distribution with a positive-definite covariance C_0 that commutes with the covariance C_1 of the target distribution, the PDF $\rho_t^\sigma(x)$ of the solution to the MGD SDE (49) satisfies*

$$\lim_{\sigma \rightarrow \infty} D_{KL}(p_1^\sigma \| p_*) = 0 \quad (50)$$

where p_* is the PDF of the maximum entropy distribution associated with the quadratic ϕ , i.e. the Gaussian distribution with mean zero and covariance $C_1 = \mathbb{E}[XX^\top]$.

Note that we make the assumption that $C_0 C_1 = C_1 C_0$ so that these two matrices are co-diagonalizable; this facilitates the proof, but the theorem remains valid if this assumption is lifted.

Proof of Theorem E.1. For the quadratic moment generating function ϕ , $\nabla \phi \nabla \phi^\top$ is a set of quadratic functions, such that

$$\begin{aligned} \mathbb{E}(\phi(X_t)) &= \mathbb{E}(\phi(I_t)) \\ \Leftrightarrow \mathbb{E}(\nabla \phi(X_t) \cdot \nabla \phi(X_t)^\top) &= \mathbb{E}((\nabla \phi(I_t) \cdot \nabla \phi(I_t)^\top)). \end{aligned}$$

In this case, MGD SDE is equal to

$$dX_t = (\eta_t^\top - \sigma^2 \theta_t^\top) \nabla \phi(X_t) dt + \sqrt{2} \sigma dW_t,$$

where

$$\begin{aligned} \mathbb{E}[\nabla \phi(I_t) \cdot \nabla \phi(I_t)^\top] \eta_t &= \mathbb{E}\left[\frac{d}{dt} I_t \nabla \phi(I_t)\right] \\ \mathbb{E}[\nabla \phi(I_t) \cdot \nabla \phi(I_t)^\top] \theta_t &= \mathbb{E}[\Delta \phi(I_t)], \end{aligned}$$

because $\Delta \phi$ is constant. Since $\mathbb{E}[\Delta \phi(I_t)] = -\mathbb{E}[\nabla \log q_t(I_t) \cdot \nabla \phi(I_t)]$, for q_t the PDF of I_t , this system is the solution to the minimisation problem

$$\begin{aligned} \eta_t &= \arg \min_{\eta} \mathbb{E}[|\eta^\top \nabla \phi(I_t) - \frac{d}{dt} I_t|^2], \\ \theta_t &= \arg \min_{\theta} \mathbb{E}[|\theta^\top \nabla \phi(I_t) + \nabla \log q_t(I_t)|^2]. \end{aligned}$$

Because $\nabla \phi$ is a set of linear functions, we can set that $\eta^\top \nabla \phi(I_t) = \tilde{\eta}^\top I_t$ and $\theta^\top \nabla \phi(I_t) = \tilde{\theta}^\top I_t$, solve for $\tilde{\eta}$ and $\tilde{\theta}$, and prove that the system's solutions are

$$\begin{aligned} \eta_t^\top \nabla \phi(x) &= \frac{1}{2} \dot{C}_t C_t^{-1} x, \\ \theta_t^\top \nabla \phi(I_t) &= C_t^{-1}(x). \end{aligned}$$

This show that MGD SDE is (49). This SDE is not a McKean Vlasov equation but a classical SDE, whose unique strong solution exists because its drift is continuous in time and Lipschitz in space. \square

Proof of Theorem E.2. Since the matrices C_0 and C_1 commute, all the matrices C_t commute. Thus, an integrating factor method shows that the solution to the MGD SDE (49) is

$$\begin{aligned} X_t &= \exp \left(\int_0^t \left(\frac{1}{2} \dot{C}_s C_s^{-1} - \sigma^2 C_s^{-1} \right) ds \right) X_0 \\ &\quad + \sqrt{2\sigma^2} \int_0^t \exp \left(\int_s^t \left(\frac{1}{2} \dot{C}_u C_u^{-1} - \sigma^2 C_u^{-1} \right) du \right) dW_s \end{aligned}$$

The conditional law of $X_t | X_0$ is gaussian, with mean $\exp \left(- \int_0^t \left(\frac{1}{2} \dot{C}_s C_s^{-1} - \sigma^2 C_s^{-1} \right) ds \right) X_0 = \mu_t X_0$ and covariance

$$\Sigma_t = 2\sigma^2 \int_0^t \exp \left(2 \int_0^s \left(\frac{1}{2} \dot{C}_u C_u^{-1} - \sigma^2 C_u^{-1} \right) du \right) ds.$$

A change of variable gives

$$\begin{aligned} \Sigma_t &= \int_0^{t\sigma^2} \exp \left(\int_0^s \left(\sigma^{-2} \frac{d}{dt} \log C_{t-u\sigma^{-2}} - 2C_{t-u\sigma^{-2}}^{-1} \right) du \right) ds \\ &= \int_0^{t\sigma^2} (C_{t-s\sigma^{-2}} C_0^{-1})^{\sigma^{-2}} \exp \left(-2 \int_0^s C_{t-u\sigma^{-2}}^{-1} du \right) ds. \end{aligned}$$

Using that C_t is bounded and has strictly positive eigenvalues, dominated convergence shows that

$$\Sigma_t \xrightarrow[\sigma \rightarrow \infty]{} 2 \int_0^\infty \exp \left(-2 \int_0^s C_t^{-1} du \right) ds = C_t.$$

A similar argument shows that

$$\mu_t \xrightarrow[\sigma \rightarrow \infty]{} 0.$$

We derive p_t^σ , the density of X_t , with the law of total probability

$$p_t^\sigma(x) = c_t \mathbb{E} \left[\exp \left(-\frac{1}{2} |\Sigma_t^{-1/2} (x - \mu_t X_0)|^2 \right) \right],$$

where $c_t = (2\pi)^{-d/2} \det(\Sigma_t)^{-1/2}$. It is straightforward with dominated convergence, with respect to X_0 for a fixed x , to show that, when σ goes to infinity

$$\begin{aligned} p_t^\sigma(x) &\xrightarrow{\text{pointwise}} p_t^*(x) \\ &\stackrel{\text{def}}{=} (2\pi)^{-d/2} \det(C_t)^{-1/2} \exp\left(-\frac{1}{2}|C_t^{-1/2}x|^2\right). \end{aligned}$$

The Kullback-Leibler divergence between p_t^σ and p_t^* is given by

$$D_{\text{KL}}(p_t^\sigma \| p_t^*) = - \int \log(p_t^\sigma(x)/p_t^*(x)) p_t^\sigma(x) dx.$$

With a change of variable,

$$\begin{aligned} & - \int \log(p_t^*(x)) p_t^\sigma(x) dx + \log((2\pi)^{d/2} \det(C_t)^{1/2}) \\ &= \int |C_t^{-1/2}x|^2 p_t^\sigma(x) dx \\ &= c_t \int |C_t^{-1/2}x|^2 e^{-\frac{1}{2}|\Sigma_t^{-1/2}(x - \mu_t x_0)|^2} p_0(x_0) dx dx_0, \\ &= c_t \int |C_t^{-1/2}(y + x_0 c'_t)|^2 e^{-\frac{1}{2}|\Sigma_t^{-1/2}y|^2} p_0(x_0) dy dx_0. \end{aligned}$$

By dominated convergence

$$\int |C_t^{-1/2}x|^2 p_t^\sigma(x) dx \xrightarrow{\sigma \rightarrow \infty} \int |C_t^{-1/2}y|^2 p_t^*(y) dy = \text{Id}.$$

and thus

$$\int \log(p_t^*(x)) p_t^\sigma(x) dx \xrightarrow{\sigma \rightarrow \infty} \log((2\pi)^{d/2} \det(C_t)^{1/2}) - \text{Id}.$$

The same dominated convergence argument is used to show that

$$\int \log(p_t^\sigma(x)) p_t^\sigma(x) dx \xrightarrow{\sigma \rightarrow \infty} \log((2\pi)^{d/2} \det(C_t)^{1/2}) - \text{Id},$$

proving that $D_{\text{KL}}(p_t^\sigma \| p_t^*)$ converges towards 0. \square

F Additional Theoretical Results

This appendix establishes rigorous existence and convergence results for the Moment Guided Diffusion (MGD) dynamics. We introduce a regularized version of MGD that includes a confining potential, which provides the analytical control needed to prove convergence to maximum entropy distributions.

F.1 Overview and Main Results

We state our two main theorems upfront, then provide detailed proofs in subsequent sections.

F.1.1 Setup and Notation

Throughout this appendix, we work with a *regularized* MGD dynamics that includes a confining potential $\frac{1}{2}\epsilon|x|^2$ for some $\epsilon > 0$. This regularization serves two purposes: (i) it ensures solutions remain well-behaved (bounded cross-entropy), and (ii) it provides a reference measure $p_\epsilon(x) = Z_\epsilon^{-1} e^{-\frac{1}{2}\epsilon|x|^2}$ with good functional inequalities.

The key objects are:

- The *cross-entropy* (negative KL divergence to reference):

$$H_\epsilon(p) = - \int p(x) \log \frac{p(x)}{p_\epsilon(x)} dx = -D_{\text{KL}}(p \| p_\epsilon)$$

- The *regularized maximum entropy distribution*:

$$p_*^\epsilon(x) = Z_*^{-1} e^{-\theta_*^\top \phi(x) - \frac{1}{2}\epsilon|x|^2}$$

satisfying $\mathbb{E}_{p_*^\epsilon}[\phi] = \mathbb{E}[\phi(X)]$

- The *Gram matrix*: $G_t = \mathbb{E}[\nabla \phi(X_t) \cdot \nabla \phi(X_t)^\top]$

Remark F.1 (Role of ϵ). *The regularization parameter $\epsilon > 0$ is held fixed throughout. The resulting limit p_* is the maximum entropy distribution with an additional Gaussian confining term. Taking $\epsilon \rightarrow 0$ would recover the unregularised maximum entropy distribution p_* , but this limit is not analysed here.*

Throughout this appendix, $|\cdot|$ will be the ℓ^2 norm of a vector with respect to coordinates (e.g. $|x| = (\sum_u |x(u)|^2)^{1/2}$ and $|\Delta \phi| = |\Delta \phi(x)| = (\sum_k |\phi_k(x)|^2)^{1/2}$) while $\|\cdot\|_\infty$ will be the ℓ^∞ norm with respect to domain and coordinates (e.g. $\|\theta_t\|_\infty = \max_{1 \leq k \leq r} |\theta_{t,k}|$ for coordinates $\theta_{t,k}$ and

$\|\nabla \phi\|_\infty = \max_{x \in \mathbb{R}^d, 1 \leq i \leq d, 1 \leq k \leq r} |\frac{\partial}{\partial x_i} \phi_k(x)|$). When specified, the ℓ^∞ can be taken with respect to a restricted domain (e.g. $\|p_t\|_{K,\infty} = \max_{x \in K} |p_t(x)|$). Finally, $\|\cdot\|_{\text{op}}$ is the operator norm of a matrix.

F.1.2 Hypotheses

We require the following regularity conditions:

Hypothesis F.2 (Regularity of ϕ). *The family of \mathcal{C}^4 functions $(\phi_k)_k$ is linearly independent and bounded, with bounded derivatives. The functions $(\nabla \phi_k)_k$ are linearly independent. For all k , the map $x \mapsto x \cdot \nabla \phi_k(x)$ is bounded.*

Hypothesis F.3 (Regularity of p_0). *The initial density p_0 is \mathcal{C}^4 , has finite variance, finite entropy, and p_0 and its derivatives are bounded.*

For the quantitative convergence result (Theorem F.7), we additionally require:

Hypothesis F.4 (Existence of p_t^*). *For all $t \in [0, 1]$, the density $p_t^*(x) = Z_{\theta_t}^{-1} e^{-\theta_t^\top \phi(x) - \frac{1}{2}\epsilon|x|^2}$ satisfying $\mathbb{E}_{p_t^*}[\phi] = m_t$ exists.*

Hypothesis F.5 (Exponential initial condition). *The initial density p_0 equals the exponential distribution p_0^* .*

F.1.3 Main Theorems

Theorem F.6 (Convergence with Fixed Moments). *Let ϕ and p_0 satisfy Hypotheses F.2 and F.3. Assume that the interpolant I_t has constant moments:*

$$\forall t \in [0, 1], \quad \frac{d}{dt} m_t = 0.$$

Then, for any $\epsilon > 0$, the strong solutions X_t of the regularized MGD (52) with PDF p_t^σ exist for all $t \in [0, 1]$ and $\sigma \in \mathbb{R}_+$.

If the density $p_^\epsilon(x) = Z_*^{-1} e^{-\theta_*^\top \phi(x) - \frac{1}{2}\epsilon|x|^2}$ with $\mathbb{E}_{p_*^\epsilon}[\phi] = \mathbb{E}[\phi(X)]$ exists, then:*

$$\lim_{\sigma \rightarrow \infty} D_{\text{KL}}(p_t^\sigma \| p_*^\epsilon) = 0.$$

Theorem F.7 (Quantitative Convergence Rate). *Assume ϕ satisfies Hypothesis F.2. Given $\epsilon > 0$, assume:*

$$\epsilon^{-1} \mathbb{E}_{p_\epsilon} [|\Delta\phi - \epsilon x \cdot \nabla\phi|^2]^{1/2} \|\nabla\phi\|_\infty < 1. \quad (51)$$

Assume p_0 satisfies Hypothesis F.5 and the interpolant I_t satisfies Hypothesis F.4.

Then there exist constants $\sigma_0, c, c' \geq 0$ such that if

$$\sigma \geq \sigma_0, \quad \max_{t \in [0, 1]} \|m_t - \mathbb{E}_{p_\epsilon}[\phi]\|_\infty \leq c, \quad \max_{t \in [0, 1]} \left\| \frac{d}{dt} m_t \right\|_\infty \leq c',$$

then solutions X_t of (52) with PDF p_t^σ exist for all $t \in [0, 1]$, and there exists $C > 0$ such that:

$$D_{\text{KL}}(p_t^\sigma \| p_t^*) \leq C\sigma^{-2}.$$

Remark F.8 (Condition (51)). *This condition ensures that the map $q_t \mapsto p_t^q$ is contractive for large σ . It requires the quantity $\Delta\phi - \epsilon x \cdot \nabla\phi$ to be sufficiently small relative to ϵ . For smooth, slowly-varying ϕ , this is typically satisfied for moderate ϵ .*

F.1.4 Proof Strategy

Theorem F.6 (Convergence with fixed moments). The proof proceeds in two stages:

Stage 1: Existence of solutions (Section F.3.1)

1. Introduce a regularized SDE with parameter $\delta > 0$ that ensures the Gram matrix $G_t + \delta I$ is invertible.
2. Show that solutions p_t^δ remain bounded in cross-entropy H_ϵ (Lemma F.13).
3. Use this bound to establish tightness (Lemma F.14) and uniform bounds on the Gram matrix (Lemma F.15).
4. Apply Kunita's theory to bound derivatives of p_t^δ (Lemma F.16).
5. Extract a convergent subsequence via Arzelà-Ascoli as $\delta \rightarrow 0$ (Lemma F.17).
6. Verify the limit satisfies the original Fokker-Planck equation (Lemma F.18).

Stage 2: Convergence to maximum entropy (Section F.3.2)

1. Show that $H_\epsilon(p_t)$ is a Lyapunov function (non-decreasing in t).
2. Extract a subsequence $t_n \rightarrow \infty$ along which the Fisher divergence vanishes (Lemma F.19).
3. Conclude D_{KL} convergence to p_*^ϵ using the Poincaré inequality (Lemmas F.20–F.21).

Theorem F.7 (Quantitative rate). This proof establishes the $O(\sigma^{-2})$ rate via a contraction argument:

1. Define the Pearson χ^2 divergence $E_t = \chi^2(p_t^\sigma \| p_t^*)$ as the key quantity.
2. Derive a differential inequality for $\frac{d}{dt} E_t$ (Lemma F.24).
3. Use the Poincaré inequality for p_t^* to control E_t (Lemma F.22).
4. Bound the perturbation $\zeta_t = \theta(q_t) - \eta(q_t)\sigma^{-2} - \theta_t^*$ in terms of E_t (Lemma F.25).
5. Show that for σ large enough, the map $q_t \mapsto p_t^q$ stabilizes a ball of radius $O(\sigma^{-2})$ (Lemma F.27).
6. Conclude existence via a fixed-point argument.

F.2 Regularized MGD Dynamics

F.2.1 Motivation: Wasserstein Gradient Flow

The Fokker-Planck equation for MGD can be interpreted as a constrained Wasserstein gradient flow. Consider maximizing the entropy $q \mapsto H(q)$ subject to the time-dependent moment constraint $\mathbb{E}_q[\phi] = m_t$. With Lagrange multipliers λ , this amounts to minimizing at each time t the functional:

$$\mathcal{F}_t(q, \lambda) = -H(q) + \lambda^\top (\mathbb{E}_q(\phi) - \mathbb{E}(\phi(I_t))).$$

The constrained Wasserstein gradient flow is:

$$\frac{\partial p_t}{\partial t} = -\nabla \cdot \left(p_t \nabla \frac{\delta \mathcal{F}_t}{\delta q}(p_t, \lambda_t) \right),$$

where λ_t is chosen to satisfy $\mathbb{E}_{p_t}(\phi) = m_t$. A calculation shows this requires:

$$\lambda_t = G_t^{-1} \left(\mathbb{E}_{p_t}[\Delta\phi] - \frac{d}{dt} m_t \right),$$

where $G_t = \mathbb{E}_{p_t}[\nabla\phi \cdot \nabla\phi^\top]$. Expanding the Wasserstein gradient flow recovers the MGD Fokker-Planck equation for $\sigma = 1$.

F.2.2 The Confined Dynamics

The existence and uniqueness of solutions to the MGD SDE is not guaranteed a priori. MGD is a McKean-Vlasov equation [33, 34] with a drift that is not Lipschitz continuous in the density p_t^σ . This can cause the Gram matrix G_t to become singular, making the drift blow up.

To ensure solutions remain regular, we replace the entropy $H(p_t^\sigma)$ with the cross-entropy relative to a Gaussian reference measure $p_\epsilon(x) = Z_\epsilon^{-1} e^{-\frac{1}{2}\epsilon|x|^2}$:

$$H_\epsilon(p_t^\sigma) = - \int p_t^\sigma(x) \log \frac{p_t^\sigma(x)}{p_\epsilon(x)} dx.$$

The maximizer of $H_\epsilon(q)$ subject to $\mathbb{E}_q[\phi] = \mathbb{E}[\phi(X)]$ is:

$$p_*^\epsilon(x) = Z_\epsilon^{-1} e^{-\theta_*^\top \phi(x) - \frac{1}{2}\epsilon|x|^2}.$$

A bounded cross-entropy ensures the solution remains regular. The corresponding Wasserstein gradient flow leads to:

Theorem F.9 (Regularized MGD). *Consider the SDE*

$$dX_t = ((\eta_t^\top - \sigma^2 \theta_t^\top) \nabla \phi(X_t) - \epsilon X_t) dt + \sqrt{2} \sigma dW_t, \quad (52)$$

where η_t and θ_t solve

$$G_t \eta_t = \frac{d}{dt} m_t, \quad (53)$$

$$G_t \theta_t = \mathbb{E}[\Delta \phi(X_t) - \epsilon X_t \nabla \phi(X_t)], \quad (54)$$

and $G_t = \mathbb{E}[\nabla \phi(X_t) \cdot \nabla \phi(X_t)^\top]$. If this coupled system admits a solution and $\mathbb{E}[\phi(X_0)] = m_0$, then:

$$\forall t \in [0, 1], \quad \mathbb{E}[\phi(X_t)] = m_t.$$

The proof follows the same argument as Theorem 3.1 in Appendix A. The term $-\epsilon X_t$ confines solutions, preventing mass from escaping to infinity.

The corresponding Fokker-Planck equation is:

$$\partial_t p_t^\sigma = \nabla \cdot (p_t(-\eta_t + \sigma^2 \theta_t)^\top \nabla \phi + \sigma^2 \epsilon x) + \sigma^2 \Delta p_t^\sigma. \quad (55)$$

F.2.3 Cross-Entropy as Lyapunov Function

When moments are fixed ($\frac{d}{dt} m_t = 0$), the cross-entropy is a Lyapunov function:

Proposition F.10. *Assume X_t with density p_t^σ follows the regularized MGD (52). If $dm_t/dt = 0$, then:*

$$\frac{d}{d\sigma} H_\epsilon(p_t^\sigma) \geq 0.$$

The proof adapts Proposition 4.3.

Remark F.11 (Non-constant moments). *When $dm_t/dt \neq 0$, the Lyapunov function becomes:*

$$\frac{d}{dt} \left(H_\epsilon(p_t^\sigma) - \int_0^t \theta_s^\top \frac{d}{ds} m_s ds \right) \geq 0.$$

However, we cannot rule out the possibility that $H(p_t^\sigma) \rightarrow -\infty$ while the integral diverges in a compensating way.

Remark F.12 (Choice of reference measure). *We use $p_\epsilon \propto e^{-\frac{1}{2}\epsilon|x|^2}$ for simplicity, but any reference measure $\propto e^{-f(x)}$ works if f grows to infinity and has a Lipschitz gradient.*

F.3 Proof of Theorem F.6: Existence and Convergence

We prove existence in Section F.3.1 and convergence in Section F.3.2.

F.3.1 Existence of Solutions

We introduce a regularized SDE with parameter $\delta > 0$, prove bounds uniform in δ , then extract a convergent subsequence as $\delta \rightarrow 0$.

Step 1: The δ -regularized dynamics. Consider the regularized SDE for $\delta > 0$ and $t \in \mathbb{R}_+$:

$$dX_t^\delta = -\left(\theta_t^\delta \nabla \phi(X_t^\delta) + \epsilon X_t^\delta\right) dt + \sqrt{2} dW_t, \quad (56)$$

where

$$\theta_t^\delta = (G_t^\delta + \delta I)^{-1} \mathbb{E}[\Delta \phi(X_t^\delta) - \epsilon X_t^\delta \cdot \nabla \phi(X_t^\delta)^\top],$$

$$\text{with } G_t^\delta = \mathbb{E}[\nabla \phi(X_t^\delta) \cdot \nabla \phi(X_t^\delta)^\top].$$

Using that $(G_t^\delta + \delta I)^{-1} \leq \delta^{-1} I$, along with Hypothesis F.2, we prove that the drift is Lipschitz in both the density of X_t^δ and space. By standard McKean-Vlasov theory, for any p_0 with finite variance, the SDE admits a unique strong solution with density p_t^δ (at least \mathcal{C}^4 by hypotheses) satisfying:

$$\partial_t p_t^\delta(x) = \nabla \cdot (p_t^\delta(\theta_t^\delta \nabla \phi(x) + \epsilon x) + \Delta p_t^\delta(x)). \quad (57)$$

Step 2: Cross-entropy bounds.

Lemma F.13 (Cross-entropy is bounded). *The relative entropy $H_\epsilon(p_t^\delta) = -\int p_t^\delta(x) \log \frac{p_t^\delta(x)}{p_\epsilon(x)} dx$ satisfies:*

$$\forall (\delta, t) \in \mathbb{R}_+^* \times \mathbb{R}_+, \quad 0 \leq -H_\epsilon(p_t^\delta) \leq -H_\epsilon(p_0).$$

Proof. Since p_0 has finite variance and entropy by hypothesis F.3, and since the drift of the SDE over X_t^δ is Lipschitz, p_t^σ admits a finite entropy and finite second order moments at each time t . It thus admits a finite cross entropy $H_\epsilon(p_t^\delta)$ at each time t .

Computing as in Proposition A,

$$\begin{aligned} \frac{d}{dt} H_\epsilon(p_t^\delta) &= -\theta_t^\delta \nabla \cdot \mathbb{E}[\Delta \phi(X_t^\delta) - \epsilon X_t^\delta \cdot \nabla \phi(X_t^\delta)] \\ &\quad + \mathbb{E}[|\nabla \log p_t^\delta(X_t^\delta) + \epsilon X_t^\delta|^2]. \end{aligned}$$

Since $H_\epsilon(p_t^\delta)$ is finite, p_t^δ is not singularly supported, so G_t^δ is invertible (as the $\nabla \phi_k$ are linearly independent). Thus, $\mathbb{E}[|\nabla \log p_t^\delta(X_t^\delta) + \epsilon X_t^\delta|^2] \geq \mathbb{E}[\Delta \phi(X_t^\delta) - \epsilon X_t^\delta \cdot \nabla \phi(X_t^\delta)^\top] G_t^\delta \mathbb{E}[\Delta \phi(X_t^\delta) - \epsilon X_t^\delta \cdot \nabla \phi(X_t^\delta)^\top]$.

Combining and using that, since $G_t^\delta \succeq 0$, we have $G_t^{\delta-1} - (G_t^\delta + \delta I)^{-1} \succeq 0$,

$$\frac{d}{dt} H_\epsilon(p_t^\delta) \geq 0. \quad \square$$

Step 3: Tightness.**Lemma F.14** (Tightness). *The family $(p_t^\delta)_{t,\delta}$ is tight:*

$$\forall \kappa > 0, \exists K \subset \mathbb{R}^d \text{ compact}, \forall t, \int_K p_t^\delta(x) dx \geq 1 - \kappa. \quad (58)$$

Proof. Apply the variational inequality $\mathbb{E}_\mu[f] \leq D_{\text{KL}}(\mu\|\nu) + \mathbb{E}_\nu[e^f]$ with $\mu = p_t^\delta, \nu = p_\epsilon, f(x) = |x|$:

$$\begin{aligned} \mathbb{E}[|X_t^\delta|] &\leq -H_\epsilon(p_t^\delta) + (2\pi\epsilon)^{-d/2} \int e^{-\frac{1}{2}\epsilon|x|^2 + |x|} dx \\ &\leq -H_\epsilon(p_0) + C_\epsilon. \end{aligned}$$

By Chebyshev's inequality, for the euclidean ball B_R with radius R

$$\int_{B_R} p_t^\delta dx \geq 1 - \frac{-H_\epsilon(p_0) + C_\epsilon}{R},$$

which exceeds $1 - \kappa$ for R large enough. \square

Step 4: Gram matrix bounds.**Lemma F.15** (Gram matrix invertibility). *Let $T > 0$ and $\delta_0 > 0$. There exists $\alpha > 0$ such that:*

$$\forall t \in [0, T], \forall \delta \in (0, \delta_0], \quad G_t^\delta \succeq \alpha I. \quad (59)$$

Consequently, $\sup_{(\delta,t) \in (0, \delta_0] \times [0, T]} \|\theta_t^\delta\|_\infty < \infty$.

Proof. The proof is by contradiction, which is equivalent to assume $\liminf_{\delta \rightarrow 0} \det G_t^\delta = 0$ for some t , since G_t^δ is bounded (Hypothesis F.2, $\nabla\phi$ is bounded). We extract $\delta_n \rightarrow 0$ such that $\det G_t^{\delta_n} \rightarrow 0$, and without loss of generality, by tightness (Lemma F.14) and Prokhorov's theorem assume that it is a weakly convergent subsequence $p_t^{\delta_n} \rightharpoonup p_\infty$.

Since $\nabla\phi$ is bounded and continuous,

$$G_t^{\delta_n} \rightarrow \mathbb{E}_{p_\infty}[\nabla\phi \cdot \nabla\phi^\top] \implies \det \mathbb{E}_{p_\infty}[\nabla\phi \cdot \nabla\phi^\top] = 0.$$

At the same time, by upper semi-continuity of cross-entropy

$$H_\epsilon(p_0) \leq \lim_n H_\epsilon(p_t^{\delta_n}) \leq H_\epsilon(p_\infty) \leq 0.$$

Thus p_∞ has finite cross-entropy, so it is not singularly supported, contradicting the singularity of $\mathbb{E}_{p_\infty}[\nabla\phi \cdot \nabla\phi^\top]$ (since $\nabla\phi_k$ are linearly independent).

The bound on θ_t^δ follows since $\Delta\phi$ and $x \mapsto x \cdot \nabla\phi(x)$ are bounded. \square

Step 5: Density bounds via Kunita's theory.**Lemma F.16** (Bounds on p_t^δ and derivatives). *The following are finite:*

$$\sup_{(\delta,t) \in (0, \delta_0] \times [0, T]} \|\nabla p_t^\delta\|_\infty < \infty, \quad (60)$$

$$\sup_{(\delta,t) \in (0, \delta_0] \times [0, T]} \|\nabla_x^2 p_t^\delta\|_\infty < \infty. \quad (61)$$

For any compact $K \subset \mathbb{R}^d$:

$$\sup_{(\delta,t) \in \mathbb{R}_+^* \times [0, T]} \|\partial_t p_t^\delta\|_{K, \infty} < \infty, \quad (62)$$

$$\sup_{(\delta,t) \in (0, \delta_0] \times [0, T]} \|\partial_t \nabla p_t^\delta\|_{K, \infty} < \infty. \quad (63)$$

Proof. The density p_t^δ follows the Feynman-Kac formula

$$p_t^\delta(x) = \mathbb{E}[\Lambda_t(x) p_0(Y_t^\delta(x))]$$

where $\Lambda_t(x) = \exp\left(-\int_0^t \nabla \cdot b_{t-s}^\delta(Y_s^\delta(x)) ds\right)$ for the Backward process $dY_s^\delta(x) = -b_{t-s}^\delta(Y_s^\delta(x)) ds + \sqrt{2}dB_s$ with $Y_0(x) = x$ and $b_t^\delta(x) = \theta_t^{\delta\top} \nabla\phi(x) + \epsilon x$. Since $\Delta\phi$ is bounded (hypothesis F.2), the divergence $\nabla \cdot b_t^\delta(x)$ is bounded, there exists C_b such that

$$\sup_{(\delta,t) \in (0, \delta_0] \times [0, T]} \|\nabla \cdot b_t^\delta\|_\infty \leq C_b.$$

Using this inequality in the Feynman-Kac formula, we prove that

$$\sup_{(\delta,t) \in (0, \delta_0] \times [0, T]} \|p_t^\delta\|_\infty \leq e^{C_b t} \|p_0\|_\infty.$$

Because $\nabla \cdot b_t^\delta$ is continuous and bounded with continuous and bounded spatial derivatives, we can use Kunita's theory to compute the derivative of $p_t^\delta(x)$ with respect to x from Feynman's Kac formula

$$\begin{aligned} \nabla p_t^\delta(x) &= \mathbb{E}\left(\Lambda_t(x) \nabla_x p_0(Y_t^\delta(x)) J_{t,t}(x)\right) \\ &\quad - \mathbb{E}\left(\int_0^t J_{t,t-s}(x) \Delta b_{t-s}^\delta(Y_s^\delta(x)) ds \Lambda_t(x) p_0(Y_t^\delta(x))\right) \end{aligned}$$

where $J_{t,s}(x) = \nabla Y_s^\delta(x)$. We derive from the SDE that

$$dJ_{t,s}(x) = -\nabla \cdot b_{t-s}^\delta(Y_s(x)) \cdot J_{t,s}(x) ds.$$

Using that $\nabla \cdot b_{t-s}^\delta$ is bounded, we prove with Grönwall's lemma, using that $J_{t,0}(x) = \text{Id}$, that

$$\forall 0 \leq s \leq t \leq T, \quad \|J_{t,s}\|_\infty \leq e^{sC_b}$$

From this inequality, and using Hypothesis F.3, we derive that

$$\sup_{(\delta,t) \in (0, \delta_0] \times [0, T]} \|\nabla p_t^\delta\|_\infty \leq e^{2TC_b} (\|\nabla p_0\|_\infty + \|p_0\|_\infty).$$

Because ϕ and Δ have bounded third and fourth order continuous derivatives, we can similarly prove that $\nabla J_{t,s}$ is bounded too, and finally that

$$\sup_{(\delta,t) \in (0, \delta_0] \times [0, T]} \|\nabla_x^2 p_t^\delta\|_\infty \leq C(\|\Delta_x p_0\|_\infty, \|\nabla p_0\|_\infty, \|p_0\|_\infty)$$

for some function $C < \infty$.

The Fokker-Planck Equation proves that $\partial_t p_t^\delta$ is bounded on any compact

$$\forall K \text{ compact} \subset \mathbb{R}^d, \exists C_K, \sup_{(\delta,t) \in \mathbb{R}_+^* \times [0,T]} \|\partial_t p_t^\delta\|_{K,\infty} \leq C_K$$

$\sup_{(\delta,t) \in (0,\delta_0] \times [0,T]} \|\partial_t \nabla p_t^\delta\|_{K,\infty}$ can be bounded with a similar argument.

□ $\mathbb{E}_{p_{t_n}} [|\nabla \log p_{t_n} + \epsilon x + \theta_\infty^\top \nabla \phi|^2] \rightarrow 0$,

$$\text{where } \theta_\infty = \mathbb{E}_{p_\infty} [\nabla \phi \cdot \nabla \phi^\top]^{-1} \mathbb{E}_{p_\infty} [\Delta \phi - \epsilon x \cdot \nabla \phi^\top].$$

Step 6: Extraction of convergent subsequence.

Lemma F.17 (Convergent subsequence). *There exist $\delta_n \rightarrow 0$ and p_t (C^2 with bounded second moment) such that:*

$$(p_t^{\delta_n}, \nabla p_t^{\delta_n}) \xrightarrow{\text{pointwise}} (p_t, \nabla p_t). \quad (64)$$

Additionally, $\mathbb{E}_{p_t} [\nabla \phi \cdot \nabla \phi^\top]$ is invertible and:

$$\theta_t^{\delta_n} \xrightarrow{\text{uniformly}} \mathbb{E}_{p_t} [\nabla \phi \cdot \nabla \phi^\top]^{-1} \mathbb{E}_{p_t} [\Delta \phi - \epsilon x \cdot \nabla \phi^\top] := \theta_t. \quad (65)$$

Proof. By Lemma F.16, p_t^δ and ∇p_t^δ are bounded and equicontinuous on $[0, T] \times K$ for any compact K . Using Arzela-Ascoli, along with a diagonal extraction argument, we can extract a subsequence $p_t^{\delta_n}$ that converges uniformly towards p_t over $[0, T] \times K$, for any compact K , which implies pointwise convergence.

Because the family is tight (Lemma F.14), dominated convergence shows that $p_t^{\delta_n}$ converges weakly towards p_t uniformly in $t \in [0, T]$, and thus that p_t is a density.

Using boundedness from Hypothesis F.2, weak convergence implies that

$$\theta_t^{\delta_n} \rightarrow \mathbb{E}_{p_t} [\nabla \phi \cdot \nabla \phi^\top]^{-1} \mathbb{E}_{p_t} [\Delta \phi - \epsilon x \cdot \nabla \phi^\top] := \theta_t$$

where $\mathbb{E}_{p_t} [\nabla \phi \nabla \phi^\top]$ is invertible because p_t has finite cross entropy. □

Step 7: The limit satisfies Fokker-Planck.

Lemma F.18 (Limit is a solution). *The limit p_t satisfies:*

$$\partial_t p_t(x) = \nabla \cdot (p_t(\theta_t^\top \nabla \phi(x) + \epsilon x)) + \Delta p_t(x), \quad (66)$$

with $\theta_t = \mathbb{E}_{p_t} [\nabla \phi \cdot \nabla \phi^\top]^{-1} \mathbb{E}_{p_t} [\Delta \phi - \epsilon x \cdot \nabla \phi^\top]$.

Proof. The density p_t^δ satisfies Duhamel's formula:

$$p_t^\delta(x) = (g_t * p_0)(x) + \int_0^t \left(g_{t-s} * \nabla (p_s^\delta(\theta_s^\delta \top \nabla \phi + \epsilon x)) \right)(x) ds,$$

where $g_t(x) = (4\pi t)^{-d/2} e^{-|x|^2/4t}$. By dominated convergence (using the bounds from Lemma F.16), the same formula holds for p_t , where θ_s^δ is replaced by θ_s . Taking the time derivative, we show that p_t satisfies the Fokker Planck equation. □

F.3.2 Convergence to Maximum Entropy

We now prove that $p_t \rightarrow p_*^\epsilon$ in D_{KL} as $\sigma \rightarrow \infty$ (equivalently, as $t \rightarrow \infty$ for fixed $\sigma = 1$, since $p_t^\sigma = p_{\sigma^2 t}^1$).

Lemma F.19 (Extraction of convergent subsequence). *There exist $t_n \rightarrow \infty$ and p_∞ (with invertible $G(p_\infty)$) such that $p_{t_n} \rightharpoonup p_\infty$ weakly and:*

$$\mathbb{E}_{p_{t_n}} [|\nabla \log p_{t_n} + \epsilon x + \theta_\infty^\top \nabla \phi|^2] \rightarrow 0,$$

$$\text{where } \theta_\infty = \mathbb{E}_{p_\infty} [\nabla \phi \cdot \nabla \phi^\top]^{-1} \mathbb{E}_{p_\infty} [\Delta \phi - \epsilon x \cdot \nabla \phi^\top].$$

Proof. Since $H_\epsilon(p_t)$ is increasing (Proposition F.10) and bounded above, it converges. Thus there exists $t_n \rightarrow \infty$ with $\frac{d}{dt} H_\epsilon(p_{t_n}) \rightarrow 0$, which equals $\mathbb{E}_{p_{t_n}} [|\nabla \log p_{t_n} + \epsilon x + \theta_{t_n}^\top \nabla \phi|^2] \rightarrow 0$.

By tightness and Prokhorov, without loss of generality, we say that $p_{t_n} \rightharpoonup p_\infty$. Upper semi-continuity gives $H_\epsilon(p_\infty) \geq \lim_n H_\epsilon(p_{t_n})$, so p_∞ has finite cross-entropy and is not singularly supported. Thus $\mathbb{E}_{p_\infty} [\nabla \phi \cdot \nabla \phi^\top]$ is invertible.

Weak convergence of p_{t_n} implies $\theta_{t_n} \rightarrow \theta_\infty$. Since the Fisher divergence vanishes along t_n and $\nabla \phi$ is bounded (Hypothesis F.2), the same holds with θ_∞ . □

Lemma F.20 (D_{KL} convergence of subsequence). *We have $\theta_\infty = \theta_*^\epsilon$ and $D_{\text{KL}}(p_{t_n} \| p_*^\epsilon) \rightarrow 0$.*

Proof. Since ϕ is bounded, $p_{\theta_\infty}(x) = Z_\infty^{-1} e^{-\theta_\infty^\top \phi(x) - \frac{1}{2} \epsilon |x|^2}$ has a bounded log-Sobolev constant c by Holley-Stroock. Thus:

$$D_{\text{KL}}(p_{t_n} \| p_{\theta_\infty}) \leq c \mathbb{E}_{p_{t_n}} [|\nabla \log p_{t_n} + \epsilon x + \theta_\infty^\top \nabla \phi|^2] \rightarrow 0.$$

The distribution p_{θ_∞} is exponential with moments $\mathbb{E}_{p_{\theta_\infty}} [\phi] = \mathbb{E}[\phi(X)]$. By uniqueness, $\theta_\infty = \theta_*^\epsilon$ and $p_{\theta_\infty} = p_*^\epsilon$. □

Lemma F.21 (Full convergence). *We have $D_{\text{KL}}(p_t \| p_*^\epsilon) \rightarrow 0$ as $t \rightarrow \infty$.*

Proof. For any weakly convergent sequence $p_{t'_n} \rightharpoonup p'_\infty$ with $t'_n \rightarrow \infty$, upper semi-continuity gives $-H_\epsilon(p'_\infty) \leq -H_\epsilon(p_*^\epsilon)$, so $p'_\infty = p_*^\epsilon$. By uniqueness of the limit in Prokhorov's theorem, $p_t \rightharpoonup p_*^\epsilon$ and $\theta_t \rightarrow \theta_*^\epsilon$.

In the expression

$$D_{\text{KL}}(p_t \| p_*^\epsilon) = -H_\epsilon(p_t) + \theta_*^{\epsilon \top} \int p_t \phi + \log Z_* Z_\epsilon^{-1},$$

each term converges, so $D_{\text{KL}}(p_t \| p_*^\epsilon) \rightarrow 0$. □

F.4 Proof of Theorem F.7: Quantitative Convergence Rate

We establish the $O(\sigma^{-2})$ rate via a contraction argument using Pearson's χ^2 divergence.

F.4.1 SDE

Let $t \mapsto q_t$ be a continuous path of densities with finite second moments. Consider the Fokker-Planck equation:

$$\partial_t p_t^q = \sigma^2 \Delta p_t^q + \sigma^2 \nabla \cdot (p_t^q (\theta(q_t) - \eta(q_t) \sigma^{-2})^\top \nabla \phi + \epsilon x), \quad (67)$$

where we defined

$$\begin{aligned} \theta(q_t) &= \mathbb{E}_{q_t} [\nabla \phi \cdot \nabla \phi^\top]^{-1} \mathbb{E}_{q_t} [\Delta \phi - \epsilon x \cdot \nabla \phi^\top], \\ \eta(q_t) &= \mathbb{E}_{q_t} [\nabla \phi \cdot \nabla \phi^\top]^{-1} \frac{d}{dt} m_t. \end{aligned} \quad (68)$$

We will show $q_t \mapsto p_t^q$ stabilizes a ball of radius $O(\sigma^{-2})$ around p_t^* in Pearson divergence.

F.4.2 Control Quantities

We define the fluctuation and Pearson divergence

$$f_t = \frac{p_t}{p_t^*} - 1, \quad E_t = \int f_t^2(x) p_t^*(x) dx = \chi^2(p_t^q \| p_t^*),$$

the parameters mismatch

$$\zeta_t = \theta(q_t) - \eta(q_t) \sigma^{-2} - \theta_t^*,$$

and constants

$$\begin{aligned} C_\Delta &= \max_{t \in [0,1]} \mathbb{E}_{p_t^*} [|\Delta \phi - \epsilon x \cdot \nabla \phi|^2]^{1/2}, \\ C_\nabla &= \mathbb{E}_{p_t^*} [|\nabla \phi|^2]^{1/2}. \end{aligned}$$

F.4.3 Poincaré Inequality

Lemma F.22 (Poincaré inequality for p_t^*). *Let $D_t = \int \|\nabla f_t\|^2 p_t^* dx$. Under Hypothesis F.2:*

$$E_t \leq \frac{1}{\lambda_*} D_t, \quad (69)$$

where $\log \lambda_* \geq \log \epsilon - \max_{t \in [0,1]} \|\theta_t^*\|_\infty \|\phi\|_\infty$.

Proof. By Holley-Stroock perturbation: p_ϵ has Poincaré constant ϵ , and $\|p_t^* - p_\epsilon\|_\infty = \|\theta_t^{*\top} \phi\|_\infty \leq \max_{t \in [0,1]} \|\theta_t^*\|_\infty \|\phi\|_\infty$. \square

F.4.4 Evolution of the Fluctuation

Lemma F.23 (Fluctuation dynamics). *The fluctuation f_t satisfies:*

$$\begin{aligned} \partial_t f_t &= \sigma^2 \mathcal{L}_t f_t + \sigma^2 \nabla \cdot ((1 + f_t) \zeta_t^\top \nabla \phi) \\ &\quad - \sigma^2 (1 + f_t) (\zeta_t^\top \nabla \phi) (\theta_t^{*\top} \nabla \phi + \epsilon x) \\ &\quad + (1 + f_t) \frac{d}{dt} \theta_t^{*\top} (\phi - m_t), \end{aligned}$$

where $\mathcal{L}_t f_t = \Delta f_t - (\theta_t^{*\top} \nabla \phi + \epsilon x) \cdot \nabla f_t$.

Proof. This is proven by a direct calculation using $p_t^q = (1 + f_t) p_t^*$ and the Fokker-Planck equation (67). \square

F.4.5 Energy Dissipation

Lemma F.24 (Pearson divergence bound). *The Pearson divergence satisfies:*

$$\begin{aligned} \frac{d}{dt} E_t &\leq -\sigma^2 \lambda_* (1 - r \max_{t \in [0,1]} \|\theta_t^*\|_\infty \|\nabla \phi\|_\infty) E_t \\ &\quad + \sigma^2 r \|\nabla \phi\|_\infty |\zeta_t|^2 (1 + E_t) \\ &\quad + 4r \max_{t \in [0,1]} \left\| \frac{d}{dt} \theta_t^* \right\|_\infty \|\phi\|_\infty (E_t^{1/2} + \frac{5}{4} E_t). \end{aligned} \quad (70)$$

Proof. We compute

$$\frac{d}{dt} E_t = 2 \int f_t \partial_t f_t p_t^* + \int f_t^2 \partial_t p_t^*.$$

Using that $\partial_t p_t^* = \frac{d}{dt} \theta_t^{*\top} (\phi - m_t) p_t^*$ The second term can be bounded by $2r \|\phi\|_\infty \max_t \|\frac{d}{dt} \theta_t^*\|_\infty E_t$ using Cauchy-Schwarz. We compute the first term on the right hand side by integrating the fluctuation evolution from Lemma F.23 multiplied by $f_t p_t^*$. We derive that

$$2\sigma^2 \int f_t (\mathcal{L}_t f_t) p_t^* = -2\sigma^2 D_t.$$

We compute the drift terms involving ζ_t . It amounts to estimate

$$\begin{aligned} I &:= 2\sigma^2 \int f_t \left(\nabla ((1 + f_t) \zeta_t^\top \nabla \phi) \right. \\ &\quad \left. - (1 + f_t) (\zeta_t^\top \nabla \phi) (\theta_t^{*\top} \nabla \phi + \epsilon x) \right) p_t^*. \end{aligned}$$

By integration by parts, we derive that

$$I = -2\sigma^2 \int (1 + f_t) (\zeta_t^\top \nabla \phi) \cdot \nabla f_t p_t^*.$$

By Cauchy-Schwarz, then using $\int (1 + f_t)^2 p_t^* = 1 + E_t$ and finally by Young's inequality,

$$\|I\| \leq \sigma^2 (\|\nabla \phi\|_\infty^2 \|\zeta_t\|^2 (1 + E_t) + D_t).$$

The remaining term in $2 \int f_t \partial_t f_t p_t^*$ satisfies

$$\begin{aligned} &|2 \int f_t (1 + f_t) \frac{d}{dt} \theta_t^{*\top} (\phi - m_t) p_t^*| \\ &\leq 4r \|\frac{d}{dt} \theta_t^*\|_\infty \|\phi\|_\infty (E_t^{1/2} + E_t) \end{aligned}$$

Combining all terms, and using the Poincaré inequality (69) to bound $-D_t$, yields (70). \square

F.4.6 Bounding ζ_t

Lemma F.25 (Control of ζ_t). *Assume $\max_t \chi^2(q_t, p_t^*) \leq E_*$. Let γ_t be the smallest eigenvalue of $G(q_t)$. Then:*

$$\gamma_t \geq \gamma_* - r^{-1} C_\nabla E_*^{1/2}, \quad (71)$$

and

$$\begin{aligned} \|\zeta_t\|_\infty^2 &\leq (\gamma_* - r^{-1} C_\nabla E_*^{1/2})^{-1} C_* E_*^{1/2} \\ &\quad + \sigma^{-2} \max_{t \in [0,1]} \left\| \frac{d}{dt} m_t \right\|_\infty, \end{aligned} \quad (72)$$

where $C_* = C_\Delta + C_\nabla \max_{t \in [0,1]} \|\theta_t^*\|_\infty$.

Proof. By Cauchy Schwarz, for any integrable g ,

$$|(\mathbb{E}_{q_t} - \mathbb{E}_{p_t^*})[g]| \leq E_*^{1/2} \int g^2 p_t^*,$$

which leads to, for the operator norm,

$$\|\mathbb{E}_{q_t}[\nabla \phi \cdot \nabla \phi^\top] - \mathbb{E}_{p_t^*}[\nabla \phi \cdot \nabla \phi^\top]\|_{\text{op}} \leq r^{-1} C_\nabla E_*^{1/2},$$

and thus to

$$\gamma_t \geq \gamma_* - r^{-1} C_\nabla E_*^{1/2}.$$

Using the constraint equation (68)

$$\begin{aligned} \mathbb{E}_{q_t}[\nabla \phi \cdot \nabla \phi^\top] \eta_t &= \\ &\quad - (\mathbb{E}_{q_t}[\nabla \phi \cdot \nabla \phi^\top] - \mathbb{E}_{p_t^*}[\nabla \phi \cdot \nabla \phi^\top]) \theta_t^* \\ &\quad - \sigma^{-2} \frac{d}{dt} m_t. \end{aligned}$$

Combining this with the Cauchy Schwarz inequality derived above, we conclude that

$$\begin{aligned} |\zeta_t| &\leq \gamma_t^{-1} \left(E_*^{1/2} C_\Delta + C_\nabla \max_{t \in [0,1]} \|\theta_t^*\|_\infty E_*^{1/2} \right. \\ &\quad \left. + \max_{t \in [0,1]} \left\| \frac{d}{dt} m_t \right\|_\infty \sigma^{-2} \right). \end{aligned}$$

□

F.4.7 Bounding Lagrange Multipliers

Lemma F.26 (Multiplier bounds). *As $m_t \rightarrow \mathbb{E}_{p_\epsilon}(\phi)$ and $\frac{d}{dt} m_t \rightarrow 0$:*

$$\begin{aligned} \theta_t^* &= O\left(\max_{t \in [0,1]} \|m_t - \mathbb{E}_{p_\epsilon}(\phi)\|_\infty\right), \\ \frac{d}{dt} \theta_t^* &= O\left(\max_{t \in [0,1]} \left\| \frac{d}{dt} m_t \right\|_\infty\right). \end{aligned} \quad (73)$$

Proof. We control $\mathbb{E}_{p_\epsilon}(\phi) - \mathbb{E}_{p_t^*}(\phi)$ with mean value theorem using that it is the gradient of $\mathcal{L}(\theta) = -\theta^\top \mathbb{E}_{p_\epsilon}(\phi) - \log Z_\theta^\epsilon$ at θ_t^* . $\mathcal{L}(\theta)$ has Hessian $-I(\theta) = -\text{Cov}_{p_\theta}(\phi)$, which is continuous and invertible (ϕ is continuous and bounded, and $\nabla \phi$ is linearly independent, see Hypothesis

F.2) and is minimised by the multiplier $\theta = 0$. Using the mean value theorem over each coordinate k of the hessian, we prove that both

$$\|\mathbb{E}_{p_\epsilon}(\phi) - \mathbb{E}_{p_t^*}(\phi)\|_\infty = O(\|I(0)\|_{\text{op}} \|\theta_t^* - 0\|_\infty),$$

$$\|\theta_t^* - 0\|_\infty = O(\|I^{-1}(0)\|_{\text{op}} \|\mathbb{E}_{p_\epsilon}(\phi) - \mathbb{E}_{p_t^*}(\phi)\|_\infty),$$

from which we deduce that

$$\theta_t^* = O\left(\max_{t \in [0,1]} \|\mathbb{E}_{p_\epsilon}(\phi) - m_t\|_\infty\right).$$

We bound the derivative $\frac{d}{dt} \theta_t^*$ by considering

$$\begin{aligned} \partial_t \nabla_\theta \mathcal{L}(\theta_t^*) &= -\frac{d}{dt} \theta_t^{*\top} I(\theta_t^*) = -\frac{d}{dt} m_t \\ &\implies \frac{d}{dt} \theta_t^* = I^{-1}(\theta_t^*) \frac{d}{dt} m_t. \end{aligned}$$

Thus, when $\frac{d}{dt} m_t \rightarrow 0$ and $m_t \rightarrow \mathbb{E}_{p_\epsilon}(\phi)$, $\frac{d}{dt} \theta_t^* = O(\max_{t \in [0,1]} \|\frac{d}{dt} m_t\|_\infty)$. □

F.4.8 Contraction

Lemma F.27 (Ball stabilization). *Assume $\max_t \chi^2(q_t, p_t^*) \leq \xi \sigma^{-2}$ for some $\xi > 0$. If $\max_{t \in [0,1]} \|m_t - \mathbb{E}_{p_\epsilon}(\phi)\|_\infty$ and $\max_{t \in [0,1]} \|\frac{d}{dt} m_t\|_\infty$ are small enough, there exists σ_0 such that for $\sigma \geq \sigma_0$:*

$$E_t \leq \xi \sigma^{-2}. \quad (74)$$

Proof. Combine Lemmas F.24 and F.25 with $E_* = \xi \sigma^{-2}$. The resulting differential inequality for E_t is a cubic polynomial in $E_t^{1/2}$. For σ large, its smallest positive root $R_* \sim \xi \sigma^{-2} \frac{C_* \|\nabla \phi\|_\infty}{A_*}$ where $A_* = \lambda_*(1 - (5\|\phi\|_\infty + \|\nabla \phi\|_\infty) \max_t \|\theta_t^*\|_\infty)$ (it can be proven by Taylor expanding, with respect to σ^{-2} , the Cardano Formula for the roots). □

By Lemmas F.22 and F.26, $\lim_{m_t \rightarrow \mathbb{E}_{p_\epsilon}(\phi)} A_* = \epsilon$ and $\lim_{m_t \rightarrow \mathbb{E}_{p_\epsilon}(\phi)} C_* = r \mathbb{E}_{p_\epsilon}[\|\Delta \phi - \epsilon x \cdot \nabla \phi\|^2]^{1/2} \|\nabla \phi\|_\infty$.

Condition (51) ensures $C_* \|\nabla \phi\|_\infty / A_* < 1$ in this limit, so $R_* \leq \xi \sigma^{-2}$ for σ large. Since the polynomial is positive on $[0, R_*]$ and $E_0 = 0$, we have $E_t \leq R_* \leq \xi \sigma^{-2}$. □

F.4.9 Conclusion

By Lemma F.27, the ball of radius $\xi \sigma^{-2}$ in Pearson divergence is stabilized by $q_t \mapsto p_t^q$. By standard McKean-Vlasov theory, a fixed point p_t^σ exists in this ball, satisfying the moment constraints. Since $\max_t \chi^2(p_t^\sigma, p_t^*) \leq \xi \sigma^{-2}$, we have $\chi^2(p_t^\sigma, p_t^*) = O(\sigma^{-2})$.

The theorem follows from $D_{\text{KL}}(p_t^\sigma \| p_t^*) \leq \chi^2(p_t^\sigma \| p_t^*)$.